Southern Ocean controls of the vertical marine $\delta^{13}C$ gradient – a modelling study

Anne L. Morée[1], Jörg Schwinger[2], Christoph Heinze[12]

[1]Geophysical Institute, University of Bergen, Bjerknes Centre for Climate Research, 5007 Bergen, Norway
[2]Uni Research Climate, Bjerknes Centre for Climate Research, 5007 Bergen, Norway

Correspondence to: Anne L. Morée (anne.moree@uib.no)

Abstract. $\delta^{13}C$, the standardised $^{13}C/^{12}C$ ratio expressed in permil, is a widely used ocean tracer to study changes in ocean circulation, water mass ventilation, atmospheric pCO_2 and the biological carbon pump on timescales ranging from decades to tens of millions of years. $\delta^{13}C$ data derived from ocean sediment core analysis provide information on $\delta^{13}C$ of dissolved inorganic carbon and the vertical $\delta^{13}C$ gradient (i.e., $\Delta\delta^{13}C$) in past oceans. In order to correctly interpret $\delta^{13}C$ and $\Delta\delta^{13}C$ variations, a good understanding is needed of the influence from ocean circulation, air-sea gas exchange and biological productivity on these variations. The Southern Ocean is a key region for these processes, and we show here that $\Delta\delta^{13}C$ in all ocean basins is sensitive to changes in the biogeochemical state of the Southern Ocean. We conduct a set of idealised sensitivity experiments with the ocean biogeochemistry general circulation model HAMOCC2s to explore the effect of biogeochemical state changes of the Southern and Global Ocean on atmospheric $\delta^{13}C$, pCO_2, and marine $\delta^{13}C$ and $\Delta\delta^{13}C$. The experiments cover changes in air-sea gas exchange rates, particulate organic carbon sinking rates, sea ice cover, and nutrient uptake efficiency - in an unchanged ocean circulation field. We conclude that the maximum variation of mean marine $\Delta\delta^{13}C$ in response to biogeochemical change is ~±0.4 ‰. However, the amplitude of this sensitivity can be higher at smaller scales, as seen from a maximum sensitivity of ~-0.6 ‰ on ocean basin scale. This local $\Delta\delta^{13}C$ sensitivity depends on local prior thermodynamic disequilibrium and the sensitivity of local POC export production to biogeochemical change. Interestingly, the direction of both glacial (intensification of $\Delta\delta^{13}C$) and interglacial (weakening of $\Delta\delta^{13}C$) $\Delta\delta^{13}C$ change matches biogeochemical processes associated with these periods. This supports the idea that biogeochemistry likely explains part of the reconstructed variations in $\Delta\delta^{13}C$, in addition to changes in ocean circulation.

1 Introduction

The vertical marine $\delta^{13}C$ gradient ($\Delta\delta^{13}C$) is the surface-to-deep difference in $\delta^{13}C$ of dissolved inorganic carbon (DIC), where the standardised $^{13}C/^{12}C$ ratio ($\delta^{13}C$) is expressed in permil (Zeebe and Wolf-Gladrow, 2001):

$$\delta^{13}C = \left(\frac{^{13}C/^{12}C}{(^{13}C/^{12}C)_{standard}} - 1\right) * 1000\ ‰. \quad (1)$$

Here, $^{13}C/^{12}C_{standard}$ is the Pee Dee Belemnite standard (0.0112372). ^{13}C is slightly heavier than the ^{12}C isotope which causes a fractionation effect during air-sea gas exchange and photosynthesis, thereby changing $\delta^{13}C$ and $\Delta\delta^{13}C$ (Laws et al., 1997;

Mackenzie and Lerman, 2006; Zhang et al., 1995). Photosynthetic fractionation increases the $^{13}C/^{12}C$ ratio of surface ocean DIC (i.e., a $\delta^{13}C$ increase) due to the preferred uptake of the lighter ^{12}C into biogenic matter (which therefore has a low $\delta^{13}C$). The deep sea DIC has a relatively low $\delta^{13}C$ signature as a result of the remineralisation of low-$\delta^{13}C$ biogenic matter at depth. The resulting vertical $\delta^{13}C$ gradient is in addition influenced by air-sea gas exchange and circulation (Emerson and Hedges, 2008; Zeebe and Wolf-Gladrow, 2001; Ziegler et al., 2013). Both deep sea and surface ocean $\delta^{13}C$ signatures are archived in the calcareous shells of foraminifera in the sediments. Records of $\delta^{13}C$ from planktic and benthic foraminiferal shell material cover tens of millions of years (Hilting et al., 2008). $\delta^{13}C$ and $\Delta\delta^{13}C$ have been used to reconstruct for example atmospheric CO_2 concentration, ocean circulation and the strength of the biological pump (Bauska et al., 2016; Broecker, 1982; Broecker and McGee, 2013; Crucifix, 2005; Curry and Oppo, 2005; Hollander and McKenzie, 1991; Hoogakker et al., 2015; Keir, 1991; Lisiecki, 2010; Oppo et al., 1990; Shackleton and Pisias, 1985; Zahn et al., 1986; Ziegler et al., 2013). Note that $\Delta\delta^{13}C$ is independent of whole-ocean $\delta^{13}C$ shifts (due to terrestrial influences) because such influences would affect $\delta^{13}C$ equally everywhere, therefore making it a valuable proxy to study the marine carbon cycle. Contemporary measurements of $\delta^{13}C$ of DIC support the quantification of anthropogenic carbon uptake by the oceans as well as the study of the effects of biology and ocean circulation on tracer distributions (Eide et al., 2017b; Gruber and Keeling, 2001; Holden et al., 2013; Kroopnick, 1980; Kroopnick, 1985; Quay et al., 2003). However, major uncertainties remain in the interpretation of foraminiferal $\delta^{13}C$ records and $\Delta\delta^{13}C$ (Broecker and McGee, 2013; Oliver et al., 2010) as well as in the interpretation of the present day $\delta^{13}C$ data (Eide et al., 2017b).

This article addresses part of these uncertainties by exploring the pre-industrial sensitivity of $\delta^{13}C$ and $\Delta\delta^{13}C$ to biogeochemical change in idealised model experiments. By doing so we can investigate a number of biogeochemical mechanisms that could explain (part of) the observed changes in $\delta^{13}C$ and $\Delta\delta^{13}C$. We focus on the Southern Ocean (SO), the ocean south of 45° S, because the SO plays an important role in the global carbon cycle by regulating atmospheric CO_2 concentrations and uptake of anthropogenic CO_2 (Broecker and Maier-Reimer, 1992; Heinze, 2002; Marinov et al., 2006) as well as influencing the global efficiency of the biological pump, global primary production and preformed nutrients (Primeau et al., 2013).

Variations in $\Delta\delta^{13}C$ over the past few 100 000 years show that $\Delta\delta^{13}C$ is generally increased during glacial periods, due to a higher contrast of deep $\delta^{13}C$ with surface and mid-depth $\delta^{13}C$ (Broecker, 1982; Boyle, 1988; Charles et al., 2010; Oliver et al., 2010; Shackleton and Pisias, 1985). Long-term $\delta^{13}C$ and $\Delta\delta^{13}C$ variations have been explained by ocean circulation changes (Duplessy et al., 1988; Jansen, 2017; Oppo et al., 1990; Toggweiler, 1999; Menviel et al., 2016). However, $\Delta\delta^{13}C$ variability cannot be explained by ocean stratification/circulation changes alone: An interaction between biogeochemical and physical processes must be at play (Boyle, 1988; Charles et al., 2010; Keir, 1991; Mulitza et al., 1998; Schmittner and Somes, 2016; Ziegler et al., 2013). $\Delta\delta^{13}C$ has been used in different ways over time: In earlier studies as the contrast between surface and deep water $\delta^{13}C$, derived from planktic versus benthic foraminifera (Boyle, 1988; Broecker, 1982; Duplessy et al., 1988; Shackleton et al., 1983) and now increasingly as the contrast of deep ocean (benthic) $\delta^{13}C$ with thermocline or intermediate ocean $\delta^{13}C$ (Charles et al., 2010; Lisiecki, 2010; Mulitza et al., 1998).

Here, we explore the sensitivity of $\delta^{13}C$ and $\Delta\delta^{13}C$ to changes in the biogeochemical state of the Global Ocean and Southern Ocean under a constant circulation field, to support the paleo-oceanographic interpretation of $\delta^{13}C$ and $\Delta\delta^{13}C$ as well to improve the understanding of the SO role in global carbon cycling and its variability and sensitivity. In order to study biogeochemical mechanisms that could influence $\delta^{13}C$ and $\Delta\delta^{13}C$, a set of sensitivity experiments is conducted with the ocean biogeochemistry general circulation model HAMOCC2s (Heinze et al., 2016). We first estimate the contribution of biology versus air-sea gas exchange to marine $\delta^{13}C$ of DIC (Sect. 3.2). The experiments focus on one or more of the biogeochemical aspects assumed to be important for $\delta^{13}C$ and $\Delta\delta^{13}C$, e.g. the biological pump efficiency and/or equilibration at the air-sea interface (Sect. 3.3.1-3.3.4). Together these experiments provide a broad spectrum of biogeochemical changes that could influence local and global $\delta^{13}C$ and $\Delta\delta^{13}C$. The modelling results of Sect. 3.3.1-3.3.4 are discussed in context of observational data from sediment cores (Sect. 3.4). As $\delta^{13}C$ and $\Delta\delta^{13}C$ are used to study changes in atmospheric pCO_2 (pCO_2^{atm}), a final section will cover the relationship between atmospheric $\delta^{13}C$, $\Delta\delta^{13}C$ and pCO_2^{atm} under different marine biogeochemical states (Sect. 3.5).

2 Methods

In this study we employ the ocean biogeochemistry general circulation model HAMOCC2s (Heinze et al., 1999; Heinze et al., 2009; Heinze et al., 2016) which simulates the inorganic and organic carbon cycle in the water column and in the sediments. The horizontal resolution of the model is 3.5° × 3.5° and there are 11 depth layers in the ocean. HAMOCC2s has an annual time step and an annually averaged fixed circulation field, as well as a free box atmosphere for O_2, $^{13}CO_2$ and CO_2. The model is computationally very economic and thus an ideal tool for sensitivity experiments over long integration times. Biogenic particulate matter in the model is represented as particulate organic carbon (POC), calcium carbonate ($CaCO_3$) and biogenic silica (opal). These biogenic particles are only modelled as export production due to the annual time-step of the model. POC and opal export production are described by Michaelis-Menten kinetics for nutrient uptake, limited by phosphate and silicic acid respectively. $CaCO_3$ export production depends on the ratio between opal and POC production. POC is carried as a tracer as well as transported downwards according to a set of mass balance equations that describe POC gain through surface layer POC production and POC losses through constant sinking and remineralisation rates (SI 1A). This is done similarly for opal and $CaCO_3$ sinking and dissolution. As the model has an annual time step, sea ice is always present south of ~60° S and north of ~70° N in the control run (Fig. S1). A more detailed model description is provided in previous studies using a similar configuration of HAMOCC2s (Heinze, 2002; Heinze et al., 2016), as well as SI 1A.

Fractionation during photosynthesis is set to a constant value of -20 ‰ (Lynch-Stieglitz et al., 1995; Tagliabue and Bopp, 2008) as model results are little influenced by the chosen parameterisation (Jahn et al., 2015; Schmittner et al., 2013). The fractionation during air-sea gas exchange depends on temperature according to $\varepsilon=-9.483*10^3/T\ [°C] + 23.89$ ‰ (Mook, 1986), causing stronger fractionation at lower temperatures (i.e. at high latitudes). Fractionation during $CaCO_3$ formation is omitted from the model as done in previous studies (Lynch-Stieglitz et al., 1995; Marchal et al., 1998; Schmittner et al., 2013) as its

size is uncertain but likely minor (~1 ‰) and effects on $\delta^{13}C$ and $\Delta\delta^{13}C$ are small (Shackleton and Pisias, 1985). In the version of HAMOCC2s used in this study, a fixed weathering input is used for ^{13}C to tune the ocean inventory to values comparable to observations. The 'best-fit' weathering value was found by running the model with a restored atmosphere ($\delta^{13}C$= -6.5 ‰) until the prognostic burial rate and weathering flux equilibrated to a constant value F_{eq}^{w} (~110000 model years). Consecutively, atmospheric restoring was removed and the weathering rate for ^{13}C was fixed to value F_{eq}^{w}. Weathering fluxes are added homogeneously over the first ocean layer as dissolved matter and in a fixed stoichiometric ratio for C, O_2, Alkalinity, PO_4^{3-} and Si. The $^{13}C/^{12}C$ ratio in the weathering flux would be equivalent to a $\delta^{13}C$ of DIC of 14 ‰. This procedure created a free atmosphere model setup with close-to-observed marine and atmospheric $\delta^{13}C$ ($\delta^{13}C^{atm}$) values. This equilibrated model version is referred to as the 'control run' in the remainder of this article. We define the vertical $\delta^{13}C$ gradient ($\Delta\delta^{13}C$) as:

$$\Delta\delta^{13}C = \delta^{13}C_{surface} - \delta^{13}C_{deep}\ , \qquad (2)$$

where $\delta^{13}C_{surface}$ and $\delta^{13}C_{deep}$ are the volume-weighted mean $\delta^{13}C$ of DIC in the surface ocean (< 50 m depth, i.e. the model photic zone) and the deep ocean (lowermost wet layer in the model, if top of layer > 3 km depth), respectively. By doing so, we can compare the $\Delta\delta^{13}C$ summarised as one number between the different sensitivity experiments.

We conducted a set of sensitivity experiments to explore changes in air-sea gas exchange rate, sea ice extent (influencing both biological production and the air-sea gas exchange of carbon) and the efficiency of the biological pump through the POC sinking rate and nutrient uptake rate (Table 1). We employ the term 'efficiency of the biological pump' as a measure of the success of phytoplankton to maintain low nutrient concentrations in the surface ocean. All experiments are run for 2000 model years starting from the end of the spinup. These runtimes allowed for atmospheric equilibrium to establish (Fig S4), with an exception for the long-term effects caused by POC sinking rate changes (as studied in more detail by Roth et al., 2014). The gas exchange rate and POC sinking rate experiments are done twice, once changing the respective model parameter for the Global Ocean and once for the Southern Ocean only (SO-only). The model parameters where changed in a way that marine biogeochemical tracer distributions (e.g. PO_4^{3-}, $\delta^{13}C$) remained reasonable but did provide an estimate of the sensitivity of the respective tracer to biogeochemical change. The model has a constant sea ice cover (Fig. S1), which permits gas and light transfer through the ice depending on ice cover fraction. The maximum and minimum sea ice cover experiments (Ice large and Ice small, Table 1) approximate the Last Glacial Maximum winter extent and the modern summer extent of SO sea ice, respectively (Crosta (2009) and Fig. A22 therein) and assume full inhibition of gas and light transfer through ice for simplicity. The experiment on nutrient drawdown (V_{max}) alters the Michaelis-Menten kinetics of POC production by changing the maximum nutrient (i.e. PO_4^{3-}) uptake rate (V_{max}^{POC} in SI 1A). The gas exchange experiments alter the specific gas exchange rate k_w as described in more detail SI 1B. The POC sinking rate experiments change the sinking velocity constant w_{POC} in the POC mass balance equations (SI 1A).

The contribution of biological processes versus air-sea gas exchange to $\delta^{13}C$ is calculated using the method of Broecker and Maier-Reimer (1992) as done for observations by Eide et al. (2017b) and in a modelling context by Sonnerup and Quay (2012):

$$\delta^{13}C_{bio}[‰] = \frac{\varepsilon_{photo}}{\overline{DIC}} * r_{c:p} * (PO_4 - \overline{PO_4}) + \overline{\delta^{13}C}\ , \quad (3)$$

where $\varepsilon_{photo} = -20$ ‰, $r_{c:p} = 122$ and the following model control run mean values are used: $\overline{DIC} = 2308.793\ \mu mol/kg$, $\overline{PO_4} = 2.399\ \mu mol/kg$ and $\overline{\delta^{13}C} = 0.742$ ‰. These values result in the modelled $\delta^{13}C_{bio}$:PO_4^{3-} relationship $\delta^{13}C_{bio}$=3.3-1.1* PO_4^{3-}. The constant 3.3 is somewhat higher than estimated for observed $\delta^{13}C$ for which a constant of 2.8 was found by Eide et al. (2017b). This higher constant originates from the over-prediction of the model of mean $\delta^{13}C$ and PO_4^{3-} at depth, as seen in other models (Sonnerup and Quay, 2012). Eq. (3) assumes a constant biological fractionation as well as a constant $r_{c:p}$ ratio, and these assumptions will introduce some error in the partition of biological and air-sea gas exchange signatures derived from observed $\delta^{13}C$ to PO_4^{3-} ratios (e.g., Eide et al. 2017b). For the purpose of determining $\delta^{13}C_{bio}$ in our model, these assumptions are unproblematic, since $r_{c:p}$ and ε_{photo} actually are taken to be constant in the model formulation. The air-sea gas signature $\delta^{13}C_{AS}$ is approximated as the residual ($\delta^{13}C_{AS} = \delta^{13}C_{model} - \delta^{13}C_{bio}$). $\delta^{13}C_{AS}$ is 0 ‰ when $\delta^{13}C_{model}=\delta^{13}C_{bio}$, i.e. when the $\delta^{13}C$ can be explained by biology only. To aid interpretation of the results, we express $\delta^{13}C_{bio}$ as a percentage as $\delta^{13}C_{bio}^{perc}$ because the absolute values in ‰ depend strongly on the chosen 'reference' values, i.e. mean DIC, PO_4^{3-}, and $\delta^{13}C$ (compare Schmittner et al., 2013; Sonnerup and Quay, 2012; Broecker and Maier-Reimer, 1992; Lynch-Stieglitz et al., 1995; Eide et al., 2017b). The conversion from $\delta^{13}C_{bio}$ to a percentage is calculated as follows:

$$\delta^{13}C_{bio}^{perc}[\%] = \frac{|\delta^{13}C_{bio}|}{|\delta^{13}C_{bio}|+|\delta^{13}C_{AS}|} * \ 100\ \% \quad (4)$$

In our analysis, we define the total amount of air-sea carbon exchange as $F_{u+d}=|F_{up}|+|F_{down}|$, with F_{up} as the upward annual carbon flux from the ocean into the atmosphere and F_{down} its downward counterpart (SI 1B and Heinze et al. (1999)). F_{u+d} is relevant for understanding the sensitivity of $\delta^{13}C$. The net carbon exchange is defined as $F_{net}=F_{up}+F_{down}$. The sign of F_{net} indicates whether a region is a source or a sink for carbon and is relevant for understanding changes in pCO_2^{atm}.

3 Results and discussion

3.1 Model control run

The model reproduces the main features of observed marine $\delta^{13}C$, as shown in Fig. 1 and Fig. S2. The modelled global mean surface ocean $\delta^{13}C_{surface}$ of DIC is higher (1.96 ‰) than deep ocean $\delta^{13}C_{deep}$ (0.76 ‰), creating a mean ocean $\Delta\delta^{13}C$ of 1.20 ‰. In the North Atlantic and SO, $\Delta\delta^{13}C$ is least pronounced (0.9 and 0.8 ‰ respectively) due to vertical mixing between surface and deep water during deep water formation and upwelling (Duplessy et al., 1988). $\Delta\delta^{13}C$ increases with water mass age as expected from the increased imprint of remineralisation on $\delta^{13}C$. The mean modelled ocean $\delta^{13}C$ is higher by 0.2 ‰ relative to observations (Eide et al., 2017b), which is especially pronounced in the oldest water masses (Fig. S2). This is observed in other models as well and attributed to the model's relative contribution of deep water production in the North Atlantic and

Southern Ocean (Sonnerup and Quay, 2012). The modelled global export POC production is 9.6 Gt C yr^{-1} of which 18 % is produced in the SO, which is within the uncertainty of observational estimates (MacCready and Quay, 2001; Nevison et al., 2012; Dunne et al., 2007; Lutz et al., 2007; Schlitzer, 2002). The free atmosphere has a modelled equilibrium pCO_2^{atm} of 279 ppm and a $\delta^{13}C^{atm}$ of -6.44 ‰ which developed in the model from the 'best-fit' weathering value F_{eq}^{w} as described above in Sect. 2. Net air-sea gas exchange is close to zero (ventilating ~5×10^{-6} Pg of carbon to the atmosphere annually), indicating that the model is in equilibrium. The resulting drift of the model control over 2000 years is +7×10^{-3} ‰ for both $\delta^{13}C^{atm}$ and mean marine $\delta^{13}C$, and +5×10^{-3} ppm for pCO_2^{atm}.

3.2 Air-sea gas exchange versus biology

The contribution of biology based on equations (2) and (3) to the $\delta^{13}C$ distribution is presented in Fig. 2, broadly in agreement with previous studies (Kroopnick, 1985; Schmittner et al., 2013). The contribution of biology to the modelled $\delta^{13}C$ distribution is generally below 45 % and has a steep gradient from the surface to the deep ocean. The (thermodynamic) fractionation effect of air-sea gas exchange on $\delta^{13}C$ is strongly impeded by the long equilibration time of ^{13}C, which results in room for biological processes to contribute significantly to $\delta^{13}C$ and $\Delta\delta^{13}C$ (Eide et al., 2017a; Lynch-Stieglitz et al., 1995; Murnane and Sarmiento, 2000; Schmittner et al., 2013). In the ocean below 250m, the influence of biology increases to 35-45 % due to the remineralisation of POC, with the exception of the Arctic Ocean where no POC production is modelled due to the sea ice cover (Fig. 2b and Fig. S1). $\delta^{13}C_{bio}^{perc}$ is close to 50 % around 1000m depth in the northern Pacific and Indian oceans, due to the old water masses located there, which have accumulated a large fraction of remineralised DIC. At the surface, air-sea gas exchange dominates the $\delta^{13}C$ signature of DIC as visible from the low $\delta^{13}C_{bio}^{perc}$ (Fig. 2a). The only exception at the surface is in upwelling regions, where a relatively high $\delta^{13}C_{bio}^{perc}$ is expected due to high POC production and upwelled remineralised carbon. High $\delta^{13}C_{bio}^{perc}$ generally corresponds to a low-$\delta^{13}C$ water mass (compare Fig. 1 and Fig. 2), as expected from the upwelling of ^{13}C-depleted DIC and modelled and observed close to the Antarctic continent (Fig. 1a and observations by Eide et al. (2017a)). The results presented in Fig. 2 appear to be quite robust as $\delta^{13}C_{bio}^{perc}$ typically does not change by more than 5-10 % for the wide range of biogeochemical states as explored in the sensitivity experiments presented below.

3.3 Sensitivity of Δδ13C and $\delta^{13}C$

3.3.1 Air-sea gas exchange of carbon

Atmospheric and marine carbon isotopic ratios are generally in thermodynamic disequilibrium because ^{13}C equilibrates ~200 times slower than inert gases like O_2. This difference in equilibration time is due to the fact that DIC needs to speciate into all marine carbon species to reach equilibrium (~20x slower than O_2), after which ^{13}C needs to go through full isotopic exchange between all carbon species to reach equilibrium (~10x slower than ^{12}C) (Jones et al., 2014; Galbraith et al., 2015; Broecker and Peng, 1974). The surface ocean $\delta^{13}C$ signature is dominated by air-sea gas exchange in most ocean regions (Fig. 2). Any change in the gas exchange rate can thus potentially have a large effect on surface ocean $\delta^{13}C$, depending on the prior

disequilibrium $\delta^{13}C_{diseq}$ ($\delta^{13}C_{diseq} = \delta^{13}C - \delta^{13}C_{eq}$, where $\delta^{13}C_{eq}$ represents the $\delta^{13}C$ value a water parcel would have had if it would have fully equilibrated with the atmosphere, see also Gruber et al. (1999)). Isotopic equilibrium with the atmosphere would result in a $\delta^{13}C_{surface}$ of approximately 2 ‰ (Murnane and Sarmiento, 2000), since $\delta^{13}C^{atm}$ is about -6.5 ‰ and air-sea fractionation about 8.5 ‰ (Mook et al., 1986).

Our gas exchange experiments (Table 1) result in a transient change in the net air-sea gas exchange flux F_{net}, which occurs until a new equilibrium is established. We find an increase of pCO_2^{atm} by 9 ppm (fast gas exchange) and by 4 ppm (slow gas exchange), respectively. If gas exchange is only changed in the SO (i.e. for 22 % of the global ice-free ocean area), an effect of 5 ppm and 1 ppm increase is found (Table 2). The spatially variable prior pCO_2 disequilibrium in the SO (Fig. S3) plays an important role in the pCO_2^{atm} sensitivity: The larger increase of the outgassing flux F_{up} of the SO as compared to the carbon uptake flux F_{down} leads to a reduced SO carbon sink and higher pCO_2^{atm} at increased gas exchange rates. The reduction in air-sea C flux for the slow gas exchange experiment causes F_{net} to decrease during the transient phase (Fig. S4 and 5), leading to an increase in pCO_2^{atm} which develops during the first ~600 years. F_{net} is reduced during the transient phase because the slow gas exchange rate decreases Southern Hemispheric net C uptake, while maintaining Northern Hemispheric net C outgassing, also for the global experiment. Interestingly, the $\delta^{13}C^{atm}$ gets decoupled from the pCO_2^{atm} signal as $\delta^{13}C^{atm}$ decreases (to -6.8 ‰) during fast gas exchange and increases (to -6.3 ‰) when the gas exchange rate is reduced. This is explained by the increase in the global amount of air-sea gas exchange F_{u+d} in the fast gas exchange experiment. Such an increase leads to a smaller thermodynamic disequilibrium, which increases the mean marine $\delta^{13}C$ and lowers $\delta^{13}C^{atm}$. Slow gas exchange reduces F_{u+d}, causing less fractionation to occur which explains the increase of $\delta^{13}C^{atm}$. Moreover, our SO-only experiments show that these effects on $\delta^{13}C^{atm}$ are more pronounced if gas exchange only changes in the SO. This indicates that the remainder of the ocean offsets part of the atmospheric sensitivity to SO change.

$\delta^{13}C$ shows a different response in high latitudes as compared to the lower latitudes in the surface ocean (Fig. 3a and S6): An increased air-sea gas exchange rate lowers the surface ocean $\delta^{13}C$ of DIC by -0.2 to -0.9 ‰ at the lower latitudes and increases surface ocean $\delta^{13}C$ at high latitudes by 0.2-0.5 ‰ (Fig. 3 and 4). These results indicate whether $\delta^{13}C_{diseq}$ is positive or negative, since $\delta^{13}C$ is closer to equilibrium at high gas exchange rates. In line with previous studies (Schmittner et al., 2013; Galbraith et al., 2015) the disequilibrium is negative ($\delta^{13}C < \delta^{13}C_{eq}$) at high latitudes and in low latitude upwelling regions, and positive elsewhere. This can be understood from the difference between the natural $\delta^{13}C$ distribution (Fig. 1) and the potential ~2 ‰ $\delta^{13}C_{eq}$, which would require an increase in $\delta^{13}C$ in cool high latitude surface waters and a decrease in warm low latitude surface waters (Murnane and Sarmiento, 2000). The net effect of a slower gas exchange rate on surface ocean $\delta^{13}C$ is less pronounced than the effect of an increased gas exchange rate (Fig. S6, Fig. 3). The smaller effects seen for slow gas exchange indicate that the control model ocean is a ‘slow ocean’, i.e. closer to (very) slow gas exchange than to thermodynamic equilibrium (fast gas exchange).

The effect of the gas exchange rate on marine $\delta^{13}C$ is mostly established in the top 250 to 1000 m of the water column (Fig. 3c, d, Fig. 4). Recording this air-sea gas exchange signal thus strongly depends on the reliability of planktic $\delta^{13}C$-based $\delta^{13}C_{surface}$ reconstructions and knowledge of the living depth represented by the planktic foraminifera. The signal penetrates

deepest (to ~2000 m depth) into the North Atlantic (Fig. 4, Fig. S7), where $\delta^{13}C$ is strongly influenced by air-sea gas exchange (Fig. 2a). However, the interpretation of variations in North Atlantic benthic $\delta^{13}C$ as coming partly from air-sea gas exchange (Lear et al., 2016) is not supported by our experiment. Due to the limited export of the $\delta^{13}C$ signal to depth, the sensitivity of $\Delta\delta^{13}C$ to the gas exchange rate mainly comes from surface ocean $\delta^{13}C$. Globally, the $\Delta\delta^{13}C$ weakens to 0.84 ‰ when the thermodynamic disequilibrium is decreased (i.e. 'Gas fast', Fig. 5) and $\Delta\delta^{13}C$ strengthens to 1.32 ‰ when the thermodynamic disequilibrium is increased ('Gas slow', Fig. 5). The extent to which thermodynamic equilibrium can develop is thus an efficient way to change the biologically-induced $\Delta\delta^{13}C$ (Murnane and Sarmiento, 2000), however only in lower latitudes where $\delta^{13}C_{diseq}$ is positive. The SO $\Delta\delta^{13}C$ signal has an opposite sign of the global mean and low latitude regions: When the thermodynamic disequilibrium is decreases (increases), basin-mean $\Delta\delta^{13}C$ in the SO increases (decreases) and thus intensifies the biologically-induced $\Delta\delta^{13}C$ changes (Fig. 4).

3.3.2 The biological pump: POC sinking rate

The net effect of a regionally changed biological pump efficiency depends on the sequestration efficiency, which depends on the interplay between the biological pump and ocean circulation (DeVries et al., 2012). A more efficient biological pump (here, a higher POC sinking rate) leads to a loss of carbon to the sediments, which affects pCO_2^{atm} and $\delta^{13}C^{atm}$ on millennial timescales. Here we present results from a 2000-year simulation (as for the other experiments), which is still in a transient phase. To reach a full equilibrium of the system could take as long as 200 000 years (Roth et al. 2014). On these long timescales other processes and feedbacks would occur (Tschumi et al. 2011), which complicates the attribution of changes to a primary trigger. A fast POC sinking rate leads to a pCO_2^{atm} decrease of 28 ppm and higher (-6.2 ‰) atmospheric $\delta^{13}C$ after 2000 years (Table 2, Fig. S5) as well as a shift of the mean ocean $\delta^{13}C$ by ~0.15 ‰, caused by the sediment burial of low-$\delta^{13}C$ POC. The imbalance between weathering and burial fluxes can thus cause profound changes in both marine and atmospheric $\delta^{13}C$, and moreover provides an important feedback for the long-term marine carbon cycle (Roth et al., 2014; Tschumi et al., 2011). In our experiment, an efficient biological pump leads to a global ~10 % decrease in the amount of air-sea gas exchange F_{u+d} because of efficient export of carbon to depth, thereby lowering the net upward advection of carbon. A mirrored but weaker response is modelled for a decrease in biological pump efficiency: Halving the POC sinking rate leads to a 13 ppm increase in pCO_2^{atm} (of which 28 % can be explained by the SO) and a more negative atmospheric $\delta^{13}C$ (-6.7 ‰) and increased F_{u+d} (Table 2, Fig. S5).

Surface ocean $\delta^{13}C$ is mostly influenced by the changes in productivity and the vertical displacement of the POC remineralisation depth. The deepening of the remineralisation depth has been extensively discussed in the literature (Boyle, 1988; Keir, 1991; Mulitza et al., 1998; Roth et al., 2014), and likely explains lowered mid-depth glacial $\delta^{13}C$ together with changes in ocean circulation (for example, Toggweiler, 1999). POC sinking removes nutrients and preferentially light ^{12}C carbon from the surface ocean, while exporting them to the deep ocean. If POC sinking rates are high, this increases the surface ocean $\delta^{13}C$ (contributing to the $\delta^{13}C^{atm}$ increase) and lowers deep ocean $\delta^{13}C$ - despite the overall increase in marine $\delta^{13}C$ which occurs due to sediment burial (Fig. 6). Therefore, even though the absolute export production is reduced in all productive

regions (-26 %), the biological pump is more efficient as any new nutrients in the surface ocean will immediately be used and exported. With a lower POC sinking rate, the remineralisation is more confined to the surface ocean. The net effect is that the surface ocean $\delta^{13}C$ becomes lower, because the fractionation effect during photosynthesis is counteracted by the remineralisation of POC (which would normally have occurred at depth). The SO plays a relatively minor role in these changes (Fig. 6b). Changes in deep ocean $\delta^{13}C$ depend on the water mass age (Fig. 6c). Old water (North Pacific) has a larger remineralisation signal when the biological pump is efficient. Independent of the biological pump efficiency, the relatively young waters of the deep North Atlantic generally adopt about the same $\delta^{13}C$ signal as the surface ocean $\delta^{13}C$, which is set by air-sea gas exchange. This is in agreement with a relatively low $\delta^{13}C_{bio}^{perc}$ estimate for the deep North Atlantic (~30 %).

The sensitivity of $\Delta\delta^{13}C$ to changes in POC sinking rate depends strongly on location (Fig. 4 and 6). In general, the $\Delta\delta^{13}C$ strengthens for an increased biological pump efficiency (Fig. 5), and this effect is stronger with water mass age (Fig. 6c, Fig. 4). The downward shift of the remineralisation depth of low-$\delta^{13}C$ POC drives this increase in $\Delta\delta^{13}C$, a mechanism discussed among others by Boyle (1988) and Mulitza et al. (1998) to understand glacial $\Delta\delta^{13}C$ increase. Our results show that the vertical displacement of the $\delta^{13}C$ profile is most pronounced in the North and South Pacific for both faster and slower POC sinking rates (Fig. 4 and Fig. S7). The North Atlantic $\Delta\delta^{13}C$ is much less affected as these waters are mostly influenced by air-sea gas exchange. Instead, the entire North Atlantic profile is shifted more than in the other ocean basins (Fig. S7). $\Delta\delta^{13}C$ weakens for a reduced biological pump efficiency (Fig. 4 and 5), especially in older water where $\delta^{13}C_{bio}^{perc}$ is higher (Fig. 2a). It is worth noting, however, that the changes in $\Delta\delta^{13}C$ in the SO are comparably small because the vertical mixing in the SO of the low-$\delta^{13}C$ deep water mostly causes shifts in the entire $\delta^{13}C$ profile, not a change in the gradient (Fig. 4).

3.3.3 The biological pump: SO nutrient depletion

Consistent with previous studies (Primeau et al., 2013; Marinov et al., 2006; Sarmiento et al., 2004), we find a large atmospheric impact of our SO nutrient depletion experiment. The high SO nutrient uptake efficiency (i.e. an efficient biological pump) causes a 51 ppm reduction in pCO_2^{atm} after 2000 years. The V_{max} experiment largely equilibrates after 800 years, as seen from the time evolution of pCO_2^{atm} and $\delta^{13}C^{atm}$ (Fig. S5). $\delta^{13}C^{atm}$ increases to -6.0 ‰ due to the increased surface ocean $\delta^{13}C$ (Fig. 7a). This 0.5 ‰ increase is high compared to the results of Menviel et al. (2015), who found a $\delta^{13}C^{atm}$ sensitivity of 0.1-0.2 ‰ in response to changes in SO nutrient utilization. The different development time as compared to the fast POC sinking rate experiment is explained by the absence of long-term loss of carbon to the sediments in the V_{max} experiment, probably because transport and water-column remineralisation within the SO limits an increase in POC burial there. In the SO, net carbon uptake (F_{net}) increases fivefold (Fig. S8) because the high nutrient and carbon consumption transport C into the ocean interior and do not permit CO_2 to escape to the atmosphere from the deep ocean.

Export production of POC is increased in the SO (Fig. S9) by a factor 2.5, causing global POC export production to increase by 17 % albeit reducing lower-latitude productivity by 11 %. This relocation of global POC export production in response to SO increased nutrient uptake efficiency is in agreement with earlier studies (Primeau et al., 2013; Marinov et al., 2006).

The increased surface ocean $\delta^{13}C$ signature everywhere north of the SO sea ice edge (Fig. 7a) is attributed to increased POC export production counteracted by a decreased F_{u+d} in the SO (which would reduce $\delta^{13}C_{surface}$ in the SO because of the negative $\delta^{13}C_{diseq}$, Fig. 3 and S6). In lower latitudes, the decreased F_{u+d} (which increases $\delta^{13}C_{surface}$ in lower latitudes because of the positive $\delta^{13}C_{diseq}$, Fig. 3 and S6) dominates the effect of the 11 % lower POC export production on $\delta^{13}C_{surface}$. At depth and under the sea ice in the Antarctic where deep water upwells, the imprint of additional POC reminneralisation at depth decreases $\delta^{13}C$ of DIC (Fig. 7). This decrease in $\delta^{13}C$ is only visible in water masses downstream of the SO (Fig.7b and c) and most pronounced in the deep North Pacific (Fig. 7c). The increased nutrient uptake rate in the SO strongly increases mean $\Delta\delta^{13}C$ (Fig. 5) and $\Delta\delta^{13}C$ in all ocean basins (Fig. 4), as seen for the fast POC sinking rate experiment. Besides effects on the $\delta^{13}C$ distribution (Fig. 7), the O_2 and PO_4^{3-} distributions change as well: The O_2 distribution is reorganised such that surface ocean O_2 is increased (up to 10 µmol kg^{-1}, with largest changes in the SO), while deep ocean O_2 is reduced downstream of the SO (up to 40 µmol kg^{-1}). Surface ocean PO_4^{3-} is reduced mostly in the SO (up to -0.8 µmol kg^{-1}). This signal is however too small to significantly increase mean deep ocean PO_4^{3-}. This implies a reduction in global preformed phosphate governed by the efficient nutrient uptake in the SO, see also Primeau et al., (2013). SO nutrient drawdown can thus cause negligible deep ocean PO_4^{3-} changes despite causing large changes in $\delta^{13}C$ and $\Delta\delta^{13}C$. This is interesting in light of glacial proxy interpretation, as deviations from the $\delta^{13}C$:PO_4^{3-} relationship (Sect. 2) are usually interpreted as the influence of air-sea gas exchange on $\delta^{13}C$ (Eide et al., 2017b; Lear et al., 2016), but could thus also come from changes in nutrient uptake efficiency. As for a changed POC sinking rate, $\Delta\delta^{13}C$ is affected more in older waters (Fig. 4).

3.3.4 Southern Ocean sea ice cover

The sea ice cover of the SO changes considerably over glacial-interglacial cycles, as well as on seasonal timescales (Crosta (2009) and Fig. A22 therein). In general, a sea ice cover will inhibit light penetration into the surface ocean as well as air-sea gas exchange. Here we assume complete inhibition of both light and air-sea carbon exchange by sea ice. In this section we thus explore the effect of both biological production and air-sea gas exchange in two extreme cases, i) the largest realistic sea ice cover based on the glacial maximum winter extreme (50° S) and ii) the smallest sea ice cover based on the contemporary summer minimum sea ice extent (70° S). Note that there is a constant sea ice cover about north of 70°N and south of 60° S in the control run of the model. Therefore, the strongest marine $\delta^{13}C$ change is expected south of 60° S for a decreased sea ice cover and between 50-60° S for an increased sea ice cover, as this is the area where ice cover is altered relative to the control run. Ocean circulation changes that could result from a changed sea ice cover are not taken into account, as we want to study the potential isolated effect of sea ice on $\delta^{13}C$ through biological and air-sea gas exchange changes.

Both local and global air-sea carbon fluxes are influenced by a change of the SO sea ice cover, which results in changes in pCO_2^{atm} and $\delta^{13}C^{atm}$. In our experiment, pCO_2^{atm} increases by 5 ppm for an increased sea ice cover and decreases by 5 ppm for a decreased sea ice cover (Table 2, Fig. S5). As noted in Sect. 3.3.1, a change in pCO_2^{atm} is governed by a transient change in the net air-sea gas exchange flux F_{net} until a new equilibrium is established. An extended ice cover causes more CO_2 to remain in the atmosphere because the additional ice covers a part of the SO that is a sink for CO_2 in the control run (Fig. S3). As the

net global air-sea gas exchange F_{net} approaches equilibrium, the non-SO ocean therefore becomes a smaller source for carbon. This reduces the net gas exchange F_{net} inside and outside of the SO by about one third. Our results show that the effects of a changed sea ice cover on pCO_2^{atm} are yet to be fully understood: Stephens and Keeling (2000) for example modelled a strong decrease of pCO_2^{atm} in response to an increased sea ice cover south of the Antarctic Polar Front, because they mostly cover a part of the SO that is a course of C to the atmosphere. In our study, the reduction in pCO_2^{atm} by 5 ppm due to a reduced sea ice cover is attributable to the POC production in the earlier ice-covered area between ~60° S and 70° S. In a sensitivity experiment where the ice cover influences air-sea gas exchange only, the sea ice retreat leads to an increase in pCO_2^{atm} because the region below the ice is strongly supersaturated in C with respect to the atmosphere. The increased sea ice cover leads to a complete suppression of air-sea gas exchange south of 50° S. Since this region is in negative carbon isotopic disequilibrium with the atmosphere ($\delta^{13}C < \delta^{13}C_{eq}$, Fig. S6), the ice cover inhibits a $\delta^{13}C$ flux into the ocean. As a result, $\delta^{13}C^{atm}$ increases to -6.1 ‰, and the opposite happens for a reduced sea ice cover, leading to a lowered $\delta^{13}C^{atm}$ (-6.6 ‰).

The increased sea ice cover over the SO results in a surface ocean $\delta^{13}C$ reduction relative to the control of -0.5 ‰ to -0.1 ‰ in the SO, while $\delta^{13}C$ is increased outside of the SO with 0-0.2 ‰ (Fig. 8a). The reduction is especially pronounced between 40-60° S. The ~40 % reduced POC export production in the SO due to light inhibition by the sea ice cover causes a major part of the SO surface $\delta^{13}C$ reduction, as the absence of photosynthesis will cause lower surface ocean $\delta^{13}C$. Next to that, the reduced air-sea gas exchange F_{u+d} in the SO also leads to a lowered surface ocean $\delta^{13}C$ signature. About the opposite happens when we simulate a strongly decreased sea ice cover (only ice south of 70° S): A small reduction of $\delta^{13}C$ is modelled outside the SO, but the SO $\delta^{13}C_{surface}$ locally becomes up to ~0.8 ‰ higher relative to the control (Fig. 8b) as the increased amount of air-sea gas exchange F_{u+d} decreases the carbon isotopic disequilibrium and increases POC production in the newly exposed area, both acting to increase $\delta^{13}C$ of DIC.

The effect of a changed ice cover on deep ocean $\delta^{13}C$ is less than ~0.1 ‰ (Fig. 8c, d) as the surface signal is diluted while it follows the general ocean circulation. As for air-sea gas exchange (Sect. 3.3.1), no pronounced deep ocean $\delta^{13}C$ signal is found outside of the SO due to sea ice cover changes (this opposed to interpretations by Lear et al., 2016). Global mean $\Delta\delta^{13}C$ is not significantly affected by changes in the SO sea ice cover (Fig. 5) because the low and high latitude effects on $\delta^{13}C_{surface}$ cancel each other out. The SO $\Delta\delta^{13}C$ however weakens considerably to 0.4 ‰ when the 50-60° S region becomes covered with sea ice and strengthens to 1 ‰ if the sea ice is removed between 60-70° S (Fig. S10). The presence or absence of a sea ice cover should thus be clearly visible in especially planktic SO $\delta^{13}C$ sediment records. The effects on $\Delta\delta^{13}C$ advance downstream of the SO, where $\Delta\delta^{13}C$ is increased up to 0.2 ‰ throughout the Pacific and Indian oceans for an increased SO sea ice cover (Fig. S10).

3.4 Modelled versus observed $\Delta\delta^{13}C$ variations

The variations in $\Delta\delta^{13}C$ on glacial-interglacial timescales provide researchers with a tracer to study the biogeochemical state of the past global ocean, under the condition that we can interpret (variations in) $\Delta\delta^{13}C$. The idealised perturbations made to the (Southern) Ocean in this study show that global mean $\Delta\delta^{13}C$ is particularly sensitive to an increased gas exchange rate and

changes in the efficiency of the biological pump. Global mean $\Delta\delta^{13}C$ varies up to ~±0.4 ‰ around the pre-industrial model reference in response to biogeochemical change (Fig. 5) - under the assumption of a constant ocean circulation. However, the sensitivity of $\Delta\delta^{13}C$ to biogeochemical changes depends strongly on location for all sensitivity experiments (Fig. 4), possibly explaining part of the incoherency of reconstructed planktic and benthic foraminiferal $\delta^{13}C$ from sediment cores (Oliver et al., 2010). In general, such $\Delta\delta^{13}C$ reconstructions show $\Delta\delta^{13}C$ variations of ~1 ‰ over the past 350 000 years (Boyle, 1988; Shackleton et al., 1983; Shackleton and Pisias, 1985; Ziegler et al., 2013; Charles et al., 2010; Oliver et al., 2010). Ocean circulation changes explain at least part of these variations in $\Delta\delta^{13}C$ (Charles et al., 2010; Heinze et al., 1991; Jansen, 2017; Heinze and Hasselmann, 1993; Oppo et al., 1990; Toggweiler 1999). However, the changes in the biogeochemical state of the ocean imposed in our experiments show that variations in $\Delta\delta^{13}C$ could be strongly influenced by (SO) biogeochemistry as well. $\Delta\delta^{13}C$ is increased during glacials and reduced during interglacials across a large set of sediment cores (Boyle, 1988; Charles et al., 2010; Oliver et al., 2010; Ziegler et al., 2013). Rapid and large changes have been documented for SO $\Delta\delta^{13}C$ records (Ziegler et al., 2013), and here we show that biogeochemical changes in the SO affect $\Delta\delta^{13}C$ globally. Our results show that an increase in mean $\Delta\delta^{13}C$ could biogeochemically result from slower gas exchange, increased POC sinking rates, or an increased nutrient uptake rate in the SO (Fig. 5). Such biogeochemical changes have been associated with glacial periods (for example, Ziegler et al. (2013)) and are potential candidates to explain part of the $\Delta\delta^{13}C$ increase in interplay with stronger ocean stratification. Sediment-core reconstructions of $\Delta\delta^{13}C$ show that an increased $\Delta\delta^{13}C$ can originate from a downward shift of the metabolic imprint of low-$\delta^{13}C$ POC which would increase shallow $\delta^{13}C$ (Boyle, 1988; Charles et al., 2010; Mulitza et al., 1998; Toggweiler, 1999), and/or a deep ocean $\delta^{13}C$ decrease (Broecker, 1982; Boyle, 1988; Oliver et al., 2010) with little variation recorded for surface ocean $\delta^{13}C$. The absence of a clear surface $\delta^{13}C$ signal could in the SO be the net effect of an increased sea ice cover (locally decreasing $\delta^{13}C$, Fig. 4 and 8a) and an increased biological pump efficiency (locally increasing $\delta^{13}C_{surface}$, Fig. 6a and b, Fig. 7a) or increased SO thermodynamic equilibrium (Fig. 3a and b) – if these opposing signals get mixed. A pronounced deep ocean $\delta^{13}C$ decrease is associated with an efficient biological pump and older water masses in our study (Fig. 4). Interestingly, large changes in deep ocean $\delta^{13}C$ and $\Delta\delta^{13}C$ do not necessarily imply changes in deep ocean PO_4^{3-} (Sect. 3.3.3). The absence of a pronounced PO_4^{3-} change despite $\Delta\delta^{13}C$ changes shows that changed ocean circulation (Toggweiler, 1999) is not the only candidate for explaining the reconstructed deepening of low-$\delta^{13}C$ water and small deep ocean glacial-interglacial PO_4^{3-} variation.

The local character of the $\Delta\delta^{13}C$ sensitivity (Fig. 4) implies that correlations between sediment core $\Delta\delta^{13}C/\delta^{13}C$ variations and global parameters (e.g. pCO_2) are not easily extrapolated to other sediment cores over large distances. Analysis of SO $\Delta\delta^{13}C$ reconstructions from sediment cores at 42° S and 46° S (Charles et al., 2010) for example shows that there is a strong correlation between these cores and Northern Hemisphere climate fluctuations. We expect that this strong correlation does not exist for cores further south in the SO because our results indicate that the SO south of ~50-60° S often has a different $\Delta\delta^{13}C$ response to biogeochemical change than the rest of the ocean.

Interglacial periods are generally thought to be associated with a decrease in the efficiency of the biological pump and increased deep-ocean ventilation via southern-sourced water masses (Gottschalk et al., 2016). Increased deep-ocean ventilation might

be driven by increased winds (Tschumi et al., 2011), which would (apart from changing the SO circulation pattern) also increase gas exchange rates. Each of these processes indeed reduces $\Delta\delta^{13}C$ in the mean in our experiments (Fig. 5), although less pronounced in the SO (Fig. 4 and Fig. S7). However, the interglacial reduction of $\Delta\delta^{13}C$ seems to originate from a deep ocean $\delta^{13}C$ increase as compared to the glacial deep ocean $\delta^{13}C$ (Broecker, 1982; Charles et al., 2010; Oliver et al., 2010). Our results show that neither an inefficient biological pump nor fast gas exchange can be associated with a pronounced deep sea $\delta^{13}C$ increase as their effects are restricted to the surface ocean. On the other hand, the interglacial decrease of $\Delta\delta^{13}C$ is a decrease as compared to the glacial state: If glacial SO nutrient uptake was higher (V_{max}), a return to the 'normal' state (i.e. the model control run) would result in a major decrease of $\Delta\delta^{13}C$ (Fig. 4 and 5).

3.5 The relationship between $\Delta\delta^{13}C$, $\delta^{13}C^{atm}$ and pCO_2^{atm}

One would expect variations of $\delta^{13}C^{atm}$ as well as $\Delta\delta^{13}C$ to correlate with variations in pCO_2^{atm}, because similar processes (biology and air-sea gas exchange) steer their distribution/concentrations (Shackleton and Pisias, 1985; this article). $\Delta\delta^{13}C$ is considered a promising proxy for reconstructions of pCO_2^{atm} for times predating ice-core records (Lisiecki, 2010). Here we show that a positive linear relationship between $\delta^{13}C^{atm}$ and global mean $\Delta\delta^{13}C$ (Fig. 9a) and a negative linear relationship between pCO_2^{atm} and global mean $\Delta\delta^{13}C$ (Fig. 9b) hold over a wide range of biogeochemical states as simulated in the sensitivity experiments. This result supports previous studies that show both local correlation between $\Delta\delta^{13}C$ and pCO_2^{atm} (such as found by for example Dickson et al. (2008)) and correlation of modified $\Delta\delta^{13}C$ between ocean basins with pCO_2^{atm} (Lisiecki, 2010). The effects of ocean circulation on glacial-interglacial $\delta^{13}C^{atm}$ changes, not studied here, are most pronounced in response to Antarctic Bottom Water formation rate variations and are of the order of 0-0.15 ‰ (Menviel et al., 2015). Our results show that $\delta^{13}C^{atm}$ varies up to ~±0.5 ‰ in response to biogeochemical changes (Table 2). Figure 9a shows that changes in the POC sinking rate lie approximately along a line in $\delta^{13}C^{atm}$:$\Delta\delta^{13}C$ space, suggesting that changes in the biological pump efficiency is important for the $\delta^{13}C^{atm}$:$\Delta\delta^{13}C$ relationship. Likewise, the relationship between pCO_2^{atm} and $\Delta\delta^{13}C$ is mostly coming from the biological pump, as air-sea gas exchange affects $\Delta\delta^{13}C$ much more than pCO_2^{atm} (Fig. 9b). Changes in air-sea gas exchange (as simulated in the gas exchange and sea ice cover experiments) affect $\delta^{13}C^{atm}$ more than $\Delta\delta^{13}C$. This confirms the idea that $\Delta\delta^{13}C$ is governed by biological processes and will also set $\delta^{13}C^{atm}$, unless air-sea gas exchange gets the chance to dominate $\delta^{13}C^{atm}$. The high potential of SO air-sea gas exchange to steer $\delta^{13}C^{atm}$ (Table 2: Sea ice and gas exchange rate experiments) complements recent studies showing that increased SO ventilation of deep ocean carbon is a likely candidate for glacial-interglacial $\delta^{13}C^{atm}$ excursions – which are of the order of 0.5 ‰ (Bauska et al., 2016; Eggleston et al., 2016; Lourantou et al., 2010; Menviel et al., 2015).

4 Summary and conclusions

This study addresses the sensitivity of modelled marine and atmospheric $\delta^{13}C$ and $\Delta\delta^{13}C$ to changes in the biogeochemical parameters under constant ocean circulation, focusing on the contribution of the SO (the ocean south of 45° S, 22 % of the

global ice-free ocean area). Variations of $\Delta\delta^{13}C$ recorded in sediment records are sensitive to ocean circulation changes as shown in previous studies, but here we show that the biogeochemical state of the (Southern) Ocean also can have large effects on $\Delta\delta^{13}C$ across all ocean basins. Using the ocean biogeochemistry general circulation model HAMOCC2s, a set of sensitivity experiments was carried out, which focuses on the biogeochemical aspects known to be important for $\delta^{13}C$ and $\Delta\delta^{13}C$. Specifically, the experiments explore changes in air-sea gas exchange rate, sea ice extent (influencing both biological production and the air-sea gas exchange of carbon) and the efficiency of the biological pump through the POC sinking rate and nutrient uptake rate.

The results show the important role of the SO in determining global $\delta^{13}C$ and $\Delta\delta^{13}C$ sensitivities, as well as the strong spatial differences in these. A new equilibrium state developed mostly within the first 100-800 years of the sensitivity experiments, except for the POC sinking experiment where an imbalance between weathering and burial causes a long-term drift. The $\delta^{13}C$ signature is governed by different processes depending on location: Air-sea gas exchange sets surface ocean $\delta^{13}C$ in all ocean basins, contributing 60-100 % to the $\delta^{13}C$ signature. At depth and with increasing water mass age, the influence of biology increases to 50 % in the oldest water masses (North Pacific) due to POC remineralisation. This spatial pattern behind the $\delta^{13}C$ signature of a water parcel results in a non-uniform sensitivity of $\delta^{13}C$ to biogeochemical change. Global mean $\Delta\delta^{13}C$ varies up to ~±0.4 ‰ due to biogeochemical state changes in our experiments (at a constant ocean circulation) (Fig. 5). This amplitude is almost half of the reconstructed variation in $\Delta\delta^{13}C$ on glacial-interglacial timescales (1 ‰), and could thus contribute to variations in $\Delta\delta^{13}C$ together with ocean circulation changes. However, $\Delta\delta^{13}C$ can have a different response on a basin scale: The ocean's oldest water (North Pacific) responds most to biological changes, the young deep water (North Atlantic) responds strongly to air-sea gas exchange changes, and the vertically well-mixed water (SO) has a low or even reversed $\Delta\delta^{13}C$ sensitivity as compared to the other basins. The amplitude of the $\Delta\delta^{13}C$ sensitivity can be higher at decreasing scale, as seen from a maximum sensitivity of ~-0.6 ‰ on ocean basin scale (Fig. 4). Interestingly, the direction of both glacial (intensification of $\Delta\delta^{13}C$) and interglacial (weakening of $\Delta\delta^{13}C$) $\Delta\delta^{13}C$ change matches changes in biogeochemical processes thought to be associated with these periods. This supports the idea that biogeochemistry explains part of the reconstructed variations in $\Delta\delta^{13}C$, in addition to changes in ocean circulation.

An increased gas exchange rate has the potential to reduce the biologically-induced $\Delta\delta^{13}C$ through the reduction of surface ocean and atmospheric $\delta^{13}C$. Increased gas exchange however only reduces $\Delta\delta^{13}C$ in the low latitudes: In high latitudes, increased gas exchange will increase $\Delta\delta^{13}C$ (by increasing $\delta^{13}C_{surface}$) because of the negative disequilibrium $\delta^{13}C_{diseq}$ (i.e. $\delta^{13}C < \delta^{13}C_{eq}$) in this region, and thus a potential to increase $\delta^{13}C_{surface}$ (section 3.3.1). pCO_2^{atm}, $\delta^{13}C^{atm}$ and marine $\delta^{13}C$ are shown to be disproportionally sensitive to SO gas exchange rate changes: The SO-only experiment results in a pCO_2^{atm} and mean $\Delta\delta^{13}C$ change as high as ~50 % of the Global experiment (for 'Gas fast').

Changes in the efficiency of the biological pump also have a major potential to alter $\Delta\delta^{13}C$ as well as pCO_2^{atm} and $\delta^{13}C^{atm}$. The globally increased POC sinking rate experiment shows that $\Delta\delta^{13}C$ strengthens in low latitudes (and more so in older waters) by deepening the low-$\delta^{13}C$ signature of remineralised POC, while SO $\Delta\delta^{13}C$ is not very sensitive to POC sinking rates. The SO effects are comparably small because the vertical mixing in the SO of the low-$\delta^{13}C$ deep water only causes shifts in the

entire $\delta^{13}C$ profile, not a change in the gradient (Fig. 4). Increased POC sinking causes a long-term imbalance between weathering and sediment burial which leads to an increase in mean $\delta^{13}C$ and $\delta^{13}C^{atm}$ (of about +0.2 ‰). Increased nutrient uptake in the SO (V_{max} experiment) results in a ~11 % lower POC export production outside of the SO, in agreement with previous studies on the role of the SO biological pump in lower latitude productivity. Interestingly, the increase of $\Delta\delta^{13}C$ in all ocean basins occurs without significantly changing deep ocean PO_4^{3-}, which advocates for increased SO nutrient uptake to explain (part of) glacial-interglacial $\Delta\delta^{13}C$ variations.

A significant linear relationship was found across the sensitivity experiments between pCO_2^{atm} and $\Delta\delta^{13}C$ as well as $\delta^{13}C^{atm}$ and $\Delta\delta^{13}C$. This result shows that paleo-reconstructions of pCO_2^{atm} based on $\Delta\delta^{13}C$ could be valid for a wide range of biogeochemical states. Such a wide applicability of a pCO_2^{atm}:$\Delta\delta^{13}C$ relationship agrees with previous studies that find pCO_2^{atm}:$\Delta\delta^{13}C$ correlation for sediment cores around the globe. The maximum response of $\delta^{13}C^{atm}$ to the biogeochemical changes imposed in our experiments (up to 0.5 ‰) is larger than the idealised maximum effect of ocean circulation changes on $\delta^{13}C^{atm}$ (0-0.15 ‰ (Menviel et al., 2015)), which underlines the potential importance of biogeochemical processes for variations in $\delta^{13}C^{atm}$. The high potential of SO air-sea gas exchange to steer $\delta^{13}C^{atm}$ (Table 2: Sea ice and gas exchange rate experiments) complements recent studies showing that increased SO ventilation of deep ocean carbon is a likely candidate for glacial-interglacial $\delta^{13}C^{atm}$ excursions.

As an outlook, the use of a more complex model with a higher horizontal and vertical resolution and a shorter time-step (resolving seasonal variations) could provide valuable additional information. For example, the role of different regions within the SO on the global $\delta^{13}C$ distribution could be better studied with a more complex model. Sediment core-based reconstructions of the global carbon cycle could possibly be aided by a more complex model with a finer grid and higher time resolution, by providing more detailed information on the contribution of biogeochemical processes to local ocean tracers. Next to that, exploring the effect on $\Delta\delta^{13}C$ of a glacial model circulation field could provide a way to quantify the maximum combined effect of circulation and biogeochemical change on $\Delta\delta^{13}C$.

Acknowledgements. The authors would like to thank two anonymous reviewer for their constructive and helpful comments, which improved this manuscript. This study is a contribution to the project “Earth system modelling of climate variations in the Anthropocene” (EVA; grant no. 229771) as well as the project “Overturning circulation and its implications for global carbon cycle in coupled models” (ORGANIC; grant no. 239965) which are both funded by the Research Council of Norway. This is a contribution to the Bjerknes Centre for Climate Research (Bergen, Norway). Storage resources were provided by the Norwegian storage infrastructure of Sigma2 (NorStore project ns2980k). Anne Morée is grateful for PhD funding through the Faculty for Mathematics and Natural Sciences of the University of Bergen and the Meltzer Foundation. Christoph Heinze acknowledges sabbatical support from the Faculty for Mathematics and Natural Sciences of the University of Bergen.

References

Bauska, T. K., Baggenstos, D., Brook, E. J., Mix, A. C., Marcott, S. A., Petrenko, V. V., Schaefer, H., Severinghaus, J. P., and Lee, J. E.: Carbon isotopes characterize rapid changes in atmospheric carbon dioxide during the last deglaciation, P Natl Acad Sci USA, 113, 3465-3470, 10.1073/pnas.1513868113, 2016.

Boyle, E. A.: The role of vertical chemical fractionation in controlling late Quaternary atmospheric carbon dioxide, Journal of Geophysical Research: Oceans, 93, 15701-15714, 10.1029/JC093iC12p15701, 1988.

Broecker, W. S.: Ocean chemistry during glacial time, Geochimica et Cosmochimica Acta, 46, 1689-1705, https://doi.org/10.1016/0016-7037(82)90110-7, 1982.

Broecker, W. S., and Maier-Reimer, E.: The influence of air and sea exchange on the carbon isotope distribution in the sea, Global Biogeochemical Cycles, 6, 315-320, 10.1029/92GB01672, 1992.

Broecker W, S., and Peng, T. H.: Gas exchange rates between air and sea, Tellus, 26, 21-35, 10.1111/j.2153-3490.1974.tb01948.x, 1974.

Broecker, W. S., and McGee, D.: The 13C record for atmospheric CO2: What is it trying to tell us?, Earth and Planetary Science Letters, 368, 175-182, http://dx.doi.org/10.1016/j.epsl.2013.02.029, 2013.

Charles, C. D., Pahnke, K., Zahn, R., Mortyn, P. G., Ninnemann, U., and Hodell, D. A.: Millennial scale evolution of the Southern Ocean chemical divide, Quaternary Science Reviews, 29, 399-409, 10.1016/j.quascirev.2009.09.021, 2010.

Crosta, X.: Antarctic Sea Ice History, Late Quaternary, in: Encyclopedia of Paleoclimatology and Ancient Environments, edited by: Gornitz, V., Springer Netherlands, Dordrecht, 31-34, 2009.

Crucifix, M.: Distribution of carbon isotopes in the glacial ocean: A model study, Paleoceanography, 20, n/a-n/a, 10.1029/2005PA001131, 2005.

Curry, W. B., and Oppo, D. W.: Glacial water mass geometry and the distribution of δ13C of ΣCO2 in the western Atlantic Ocean, Paleoceanography, 20, n/a-n/a, 10.1029/2004PA001021, 2005.

DeVries, T., Primeau, F., and Deutsch, C.: The sequestration efficiency of the biological pump, Geophysical Research Letters, 39, L13601, 10.1029/2012GL051963, 2012.

Dickson, A. J., Leng, M. J., and Maslin, M. A.: Mid-depth South Atlantic Ocean circulation and chemical stratification during MIS-10 to 12: implications for atmospheric CO2, Clim. Past, 4, 333-344, 10.5194/cp-4-333-2008, 2008.

Dunne, J. P., Sarmiento, J. L., and Gnanadesikan, A.: A synthesis of global particle export from the surface ocean and cycling through the ocean interior and on the seafloor, Global Biogeochemical Cycles, 21, GB4006, 10.1029/2006GB002907, 2007.

Duplessy, J. C., Shackleton, N. J., Fairbanks, R. G., Labeyrie, L., Oppo, D., and Kallel, N.: Deepwater source variations during the last climatic cycle and their impact on the global deepwater circulation, Paleoceanography, 3, 343-360, 10.1029/PA003i003p00343, 1988.

Eggleston, S., Schmitt, J., Bereiter, B., Schneider, R., and Fischer, H.: Evolution of the stable carbon isotope composition of atmospheric CO2 over the last glacial cycle, Paleoceanography, 31, 434-452, 10.1002/2015PA002874, 2016.

Eide, M., Olsen, A., Ninnemann, U. S., and Eldevik, T.: A global estimate of the full oceanic 13C Suess effect since the preindustrial, Global Biogeochemical Cycles, 31, 492-514, 10.1002/2016GB005472, 2017a.

Eide, M., Olsen, A., Ninnemann, U. S., and Johannessen, T.: A global ocean climatology of preindustrial and modern ocean δ13C, Global Biogeochemical Cycles, 31, 515-534, 10.1002/2016GB005473, 2017b.

Emerson, S., and Hedges, J.: Chemical oceanography and the marine carbon cycle, Cambridge University Press, Cambridge, xi, 453 p. 458 p. of col. plates pp., 2008.

Galbraith, E. D., Kwon, E. Y., Bianchi, D., Hain, M. P., and Sarmiento, J. L.: The impact of atmospheric pCO_2 on carbon isotope ratios of the atmosphere and ocean, Global Biogeochemical Cycles, 29, 307-324, 10.1002/2014GB004929, 2015.

Gottschalk, J., Skinner, L. C., Lippold, J., Vogel, H., Frank, N., Jaccard, S. L., and Waelbroeck, C.: Biological and physical controls in the Southern Ocean on past millennial-scale atmospheric CO2 changes, 7, 11539, 10.1038/ncomms11539 https://www.nature.com/articles/ncomms11539#supplementary-information, 2016.

Gruber, N., Keeling, C. D., Bacastow, R. B., Guenther, P. R., Lueker, T. J., Wahlen, M., Meijer, H. A. J., Mook, W. G., and Stocker, T. F.: Spatiotemporal patterns of carbon-13 in the global surface oceans and the oceanic suess effect, Global Biogeochemical Cycles, 13, 307-335, doi:10.1029/1999GB900019, 1999.

Gruber, N., and Keeling, C. D.: An improved estimate of the isotopic air-sea disequilibrium of CO2: Implications for the oceanic uptake of anthropogenic CO2, Geophysical Research Letters, 28, 555-558, 10.1029/2000GL011853, 2001.

Heinze, C., Maier-Reimer, E., and Winn, K.: Glacial pCO_2 Reduction by the World Ocean: Experiments With the Hamburg Carbon Cycle Model, Paleoceanography, 6, 395-430, 10.1029/91PA00489, 1991.
Heinze, C., and Hasselmann, K.: Inverse Multiparameter Modeling of Paleoclimate Carbon Cycle Indices, Quaternary Research, 40, 281-296, https://doi.org/10.1006/qres.1993.1082, 1993.
Heinze, C., and Maier-Reimer, E.: The Hamburg Oceanic Carbon Cycle Circulation Model Version "HAMOCC2s" for long time integrations, Max-Planck-Institut für Meteorologie, Hamburg REPORT 20, 1999.
Heinze, C.: Assessing the importance of the Southern Ocean for natural atmospheric pCO_2 variations with a global biogeochemical general circulation model, Deep Sea Research Part II: Topical Studies in Oceanography, 49, 3105-3125, http://dx.doi.org/10.1016/S0967-0645(02)00074-7, 2002.
Heinze, C., Hoogakker, B. A. A., and Winguth, A.: Ocean carbon cycling during the past 130 000 years – a pilot study on inverse palaeoclimate record modelling, Clim. Past, 12, 1949-1978, 10.5194/cp-12-1949-2016, 2016.
Hilting, A. K., Kump, L. R., and Bralower, T. J.: Variations in the oceanic vertical carbon isotope gradient and their implications for the Paleocene-Eocene biological pump, Paleoceanography, 23, n/a-n/a, 10.1029/2007PA001458, 2008.
Holden, P. B., Edwards, N. R., Müller, S. A., Oliver, K. I. C., Death, R. M., and Ridgwell, A.: Controls on the spatial distribution of oceanic δ13C_DIC, Biogeosciences, 10, 1815-1833, 10.5194/bg-10-1815-2013, 2013.
Hollander, D. J., and McKenzie, J. A.: CO2 control on carbon-isotope fractionation during aqueous photosynthesis: A paleo-pCO_2 barometer, Geology, 19, 929-932, 10.1130/0091-7613(1991)019<0929:ccocif>2.3.co;2, 1991.
Hoogakker, B. A. A., Elderfield, H., Schmiedl, G., McCave, I. N., and Rickaby, R. E. M.: Glacial-interglacial changes in bottom-water oxygen content on the Portuguese margin, Nature Geosci, 8, 40-43, 10.1038/ngeo2317 http://www.nature.com/ngeo/journal/v8/n1/abs/ngeo2317.html#supplementary-information, 2015.
Jahn, A., Lindsay, K., Giraud, X., Gruber, N., Otto-Bliesner, B. L., Liu, Z., and Brady, E. C.: Carbon isotopes in the ocean model of the Community Earth System Model (CESM1), Geoscientific Model Development, 8, 2419-2434, 10.5194/gmd-8-2419-2015, 2015.
Jansen, M. F.: Glacial ocean circulation and stratification explained by reduced atmospheric temperature, Proceedings of the National Academy of Sciences, 114, 45-50, 10.1073/pnas.1610438113, 2017.
Jones, D. C., Ito, T., Takano, Y., and Hsu, W.-C.: Spatial and seasonal variability of the air-sea equilibration timescale of carbon dioxide, Global Biogeochemical Cycles, 28, 1163-1178, 10.1002/2014GB004813, 2014.
Keir, R. S.: The effect of vertical nutrient redistribution on surface ocean δ13C, Global Biogeochemical Cycles, 5, 351-358, doi:10.1029/91GB01913, 1991.
Kroopnick, P.: The distribution of 13C in the Atlantic Ocean, Earth and Planetary Science Letters, 49, 469-484, https://doi.org/10.1016/0012-821X(80)90088-6, 1980.
Kroopnick, P. M.: The distribution of 13C of ΣCO2 in the world oceans, Deep Sea Research Part A. Oceanographic Research Papers, 32, 57-84, https://doi.org/10.1016/0198-0149(85)90017-2, 1985.
Laws, E. A., Bidigare, R., R., and Popp, B. N.: Effects of growth rate and CO2 concentration on carbon isotopic fractionation by the marine diatom Phaeodactylum tricornutum, Limnol. Oceanogr., 42, 1552-1560, 1997.
Lear, C. H., Billups, K., Rickaby, R. E. M., Diester-Haass, L., Mawbey, E. M., and Sosdian, S. M.: Breathing more deeply: Deep ocean carbon storage during the mid-Pleistocene climate transition, Geology, 44, 1035-1038, 10.1130/G38636.1, 2016.
Lisiecki, L. E.: A benthic δ13C-based proxy for atmospheric pCO2 over the last 1.5 Myr, Geophysical Research Letters, 37, 10.1029/2010GL045109, 2010.
Lourantou, A., Lavrič Jošt, V., Köhler, P., Barnola, J. M., Paillard, D., Michel, E., Raynaud, D., and Chappellaz, J.: Constraint of the CO2 rise by new atmospheric carbon isotopic measurements during the last deglaciation, Global Biogeochemical Cycles, 24, 10.1029/2009GB003545, 2010.
Lutz, M. J., Caldeira, K., Dunbar, R. B., and Behrenfeld, M. J.: Seasonal rhythms of net primary production and particulate organic carbon flux to depth describe the efficiency of biological pump in the global ocean, Journal of Geophysical Research: Oceans, 112, C10011, 10.1029/2006JC003706, 2007.
Lynch-Stieglitz, J., Stocker, T. F., Broecker, W. S., and Fairbanks, R. G.: The influence of air-sea exchange on the isotopic composition of oceanic carbon: Observations and modeling, Global Biogeochemical Cycles, 9, 653-665, 10.1029/95GB02574, 1995.

MacCready, P., and Quay, P.: Biological export flux in the Southern Ocean estimated from a climatological nitrate budget, Deep Sea Research Part II: Topical Studies in Oceanography, 48, 4299-4322, http://dx.doi.org/10.1016/S0967-0645(01)00090-X, 2001.

Mackenzie, F. T., and Lerman, A.: Isotopic Fractionation of Carbon: Inorganic and Biological Processes, in: Carbon in the Geobiosphere — Earth's Outer Shell —, edited by: Mackenzie, F. T., and Lerman, A., Springer Netherlands, Dordrecht, 165-191, 2006.

Marchal, O., Stocker, T. F., and Joos, F.: A latitude-depth, circulation-biogeochemical ocean model for paleoclimate studies. Development and sensitivities, Tellus B, 50, 290-316, 10.1034/j.1600-0889.1998.t01-2-00006.x, 1998.

Marinov, I., Gnanadesikan, A., Toggweiler, J. R., and Sarmiento, J. L.: The Southern Ocean biogeochemical divide, Nature, 441, 964-967, http://www.nature.com/nature/journal/v441/n7096/suppinfo/nature04883.html, 2006.

Menviel, L., Mouchet, A., Meissner, K. J., Joos, F., and England, M. H.: Impact of oceanic circulation changes on atmospheric δ13CO2, Global Biogeochemical Cycles, 29, 1944-1961, 10.1002/2015GB005207, 2015.

Menviel, L., Yu, J., Joos, F., Mouchet, A., Meissner, K. J., and England, M. H.: Poorly ventilated deep ocean at the Last Glacial Maximum inferred from carbon isotopes: A data-model comparison study, Paleoceanography, 32, 2-17, 10.1002/2016PA003024, 2016.

Mook, W. G.: 13C in atmospheric CO2, Netherlands Journal of Sea Research, 20, 211-223, http://dx.doi.org/10.1016/0077-7579(86)90043-8, 1986.

Mulitza, S., Rühlemann, C., Bickert, T., Hale, W., Pätzold, J., and Wefer, G.: Late Quaternary δ13C gradients and carbonate accumulation in the western equatorial Atlantic, Earth and Planetary Science Letters, 155, 237-249, https://doi.org/10.1016/S0012-821X(98)00012-0, 1998.

Murnane, R. J., and Sarmiento, J. L.: Roles of biology and gas exchange in determining the δ13C distribution in the ocean and the preindustrial gradient in atmospheric δ13C, Global Biogeochemical Cycles, 14, 389-405, 10.1029/1998GB001071, 2000.

Nevison, C. D., Keeling, R. F., Kahru, M., Manizza, M., Mitchell, B. G., and Cassar, N.: Estimating net community production in the Southern Ocean based on atmospheric potential oxygen and satellite ocean color data, Global Biogeochemical Cycles, 26, GB1020, 10.1029/2011GB004040, 2012.

Oliver, K. I. C., Hoogakker, B. A. A., Crowhurst, S., Henderson, G. M., Rickaby, R. E. M., Edwards, N. R., and Elderfield, H.: A synthesis of marine sediment core δ13C data over the last 150 000 years, Climate of the Past, 6, 645-673, 2010.

Oppo, D. W., Fairbanks, R. G., and Gordon, A. L.: Late Pleistocene Southern Ocean δ13C variability, Paleoceanography, 5, 43-54, 10.1029/PA005i001p00043, 1990.

Primeau, F. W., Holzer, M., and DeVries, T.: Southern Ocean nutrient trapping and the efficiency of the biological pump, Journal of Geophysical Research: Oceans, 118, 2547-2564, 10.1002/jgrc.20181, 2013.

Quay, P., Sonnerup, R., Westby, T., Stutsman, J., and McNichol, A.: Changes in the 13C/12C of dissolved inorganic carbon in the ocean as a tracer of anthropogenic CO2 uptake, Global Biogeochemical Cycles, 17, 4-1-4-20, 10.1029/2001GB001817, 2003.

Roth, R., Ritz, S. P., and Joos, F.: Burial-nutrient feedbacks amplify the sensitivity of atmospheric carbon dioxide to changes in organic matter remineralisation, Earth Syst Dynam, 5, 321-343, 10.5194/esd-5-321-2014, 2014.

Sarmiento, J. L., Gruber, N., Brzezinski, M. A., and Dunne, J. P.: High-latitude controls of thermocline nutrients and low latitude biological productivity, Nature, 427, 56-60, 2004.

Schlitzer, R.: Carbon Export Fluxes in the Southern Ocean: Results from Inverse Modeling and Comparison with Satellite Estimates, Deep Sea Research, 2, 1623-1644, 2002.

Schmittner, A., Gruber, N., Mix, A. C., Key, R. M., Tagliabue, A., and Westberry, T. K.: Biology and air-sea gas exchange controls on the distribution of carbon isotope ratios (δ13C) in the ocean, Biogeosciences, 10, 5793-5816, 10.5194/bg-10-5793-2013, 2013.

Schmittner, A., and Somes, C. J.: Complementary constraints from carbon (13C) and nitrogen (15N) isotopes on the glacial ocean's soft-tissue biological pump, Paleoceanography, 31, 669-693, 10.1002/2015PA002905, 2016.

Shackleton, N. J., Hall, M. A., Line, J., and Shuxi, C.: Carbon isotope data in core V19-30 confirm reduced carbon dioxide concentration in the ice age atmosphere, Nature, 306, 319, 10.1038/306319a0, 1983.

Shackleton, N. J., and Pisias, N. G.: Atmospheric carbon dioxide, orbital forcing, and climate, in: The Carbon cycle and atmospheric CO2: natural variations archean to present, edited by: Sundquist, E. T., and Broecker, W. S., Geophysical Monograph, American Geophysical Union, Washington, 303-317, 1985.

Sonnerup, R. E., and Quay, P. D.: 13C constraints on ocean carbon cycle models, Global Biogeochemical Cycles, 26, GB2014, 10.1029/2010GB003980, 2012.
Stephens, B. B., and Keeling, R. F.: The influence of Antarctic sea ice on glacial–interglacial CO2 variations, Nature, 404, 171, 10.1038/35004556, 2000.
Tagliabue, A., and Bopp, L.: Towards understanding global variability in ocean carbon-13, Global Biogeochemical Cycles, 22, GB1025, 10.1029/2007GB003037, 2008.
Toggweiler, J. R.: Variation of atmospheric CO2 by ventilation of the ocean's deepest water, Paleoceanography, 14, 571-588, 10.1029/1999PA900033, 1999.
Tschumi, T., Joos, F., Gehlen, M., and Heinze, C.: Deep ocean ventilation, carbon isotopes, marine sedimentation and the deglacial CO2 rise, Clim. Past, 7, 771-800, https://doi.org/10.5194/cp-7-771-2011, 2011.
Zahn, R., Winn, K., and Sarnthein, M.: Benthic foraminiferal δ13C and accumulation rates of organic carbon: Uvigerina Peregrina group and Cibicidoides Wuellerstorfi, Paleoceanography, 1, 27-42, 10.1029/PA001i001p00027, 1986.
Zeebe, R., and Wolf-Gladrow, D.: CO2 in Seawater: Equilibrium, Kinetics, Isotopes, Elsevier Oceanography Series, edited by: Halpern, D., Elsevier Science B.V., Amsterdam, The Netherlands, 346 pp., 2001.
Zhang, J., Quay, P. D., and Wilbur, D. O.: Carbon isotope fractionation during gas-water exchange and dissolution of CO2, Geochimica et Cosmochimica Acta, 59, 107-114, http://dx.doi.org/10.1016/0016-7037(95)91550-D, 1995.
Ziegler, M., Diz, P., Hall, I. R., and Zahn, R.: Millennial-scale changes in atmospheric CO2 levels linked to the Southern Ocean carbon isotope gradient and dust flux, Nature Geosci, 6, 457-461, 10.1038/ngeo1782 http://www.nature.com/ngeo/journal/v6/n6/abs/ngeo1782.html#supplementary-information, 2013.

Experiment	Experiment setup
Gas fast	CO_2 gas exchange rate * 4
Gas slow	CO_2 gas exchange rate / 4
Efficient biological pump	POC sinking rate doubled to 6m/d
Inefficient biological pump	POC sinking rate halved to 1.5m/d
V_{max}	High nutrient uptake rate (control*5) in the Southern Ocean
Ice large	Southern Ocean sea ice cover south of 50° S
Ice small	Southern Ocean sea ice cover south of 70° S

Table 1 Description of the sensitivity experiments. The sensitivity experiments on the CO_2 gas exchange rate and the biological pump have been done twice, once for the Global Ocean and once only making changes in the Southern Ocean (south of 45° S).

	Global experiments		SO-only experiments	
	pCO_2^{atm}	$\delta^{13}C^{atm}$	pCO_2^{atm}	$\delta^{13}C^{atm}$
Control	279	-6,4	-	
Gas exchange				
Fast	288	-6,8	284	-6,9
Slow	284	-6,3	281	-6,1
Biological pump				
POC: Efficient	252	-6,2	275	-6,4
POC: Inefficient	293	-6,7	283	-6,5
V_{max}	-		229	-6,0
Ice				
Large	-		284	-6,1
Small	-		274	-6,6

Table 2 Results of pCO_2^{atm} [ppm] and $\delta^{13}C^{atm}$ [‰] for all sensitivity experiments.

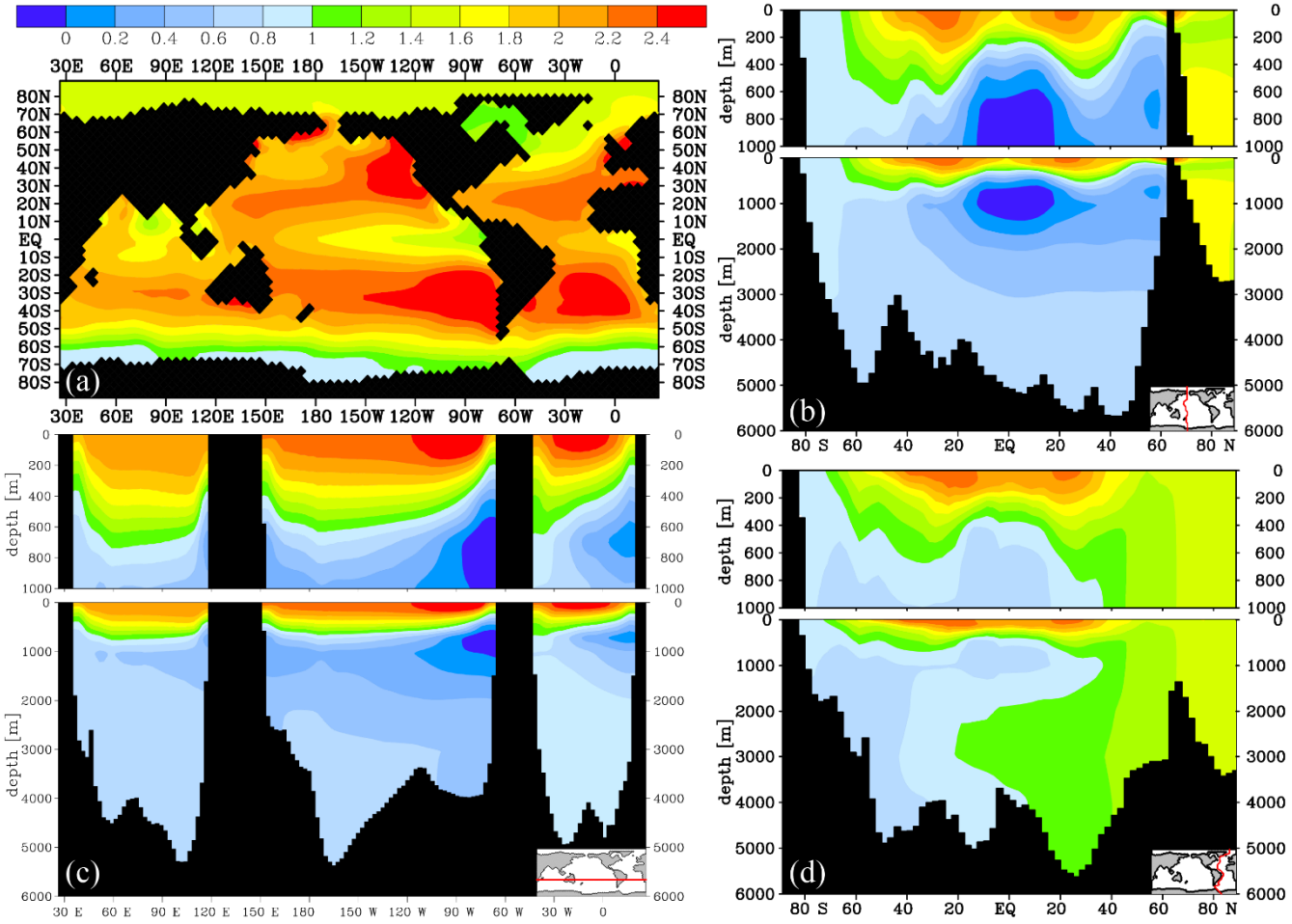

Figure 1 Modelled $\delta^{13}C$ of DIC [‰] distribution for the model control run: (a) $\delta^{13}C$ at 25 m depth, (b) Pacific transect of $\delta^{13}C$, (c) Zonal transect of $\delta^{13}C$ at 26° S, and (d) Atlantic transect of $\delta^{13}C$.

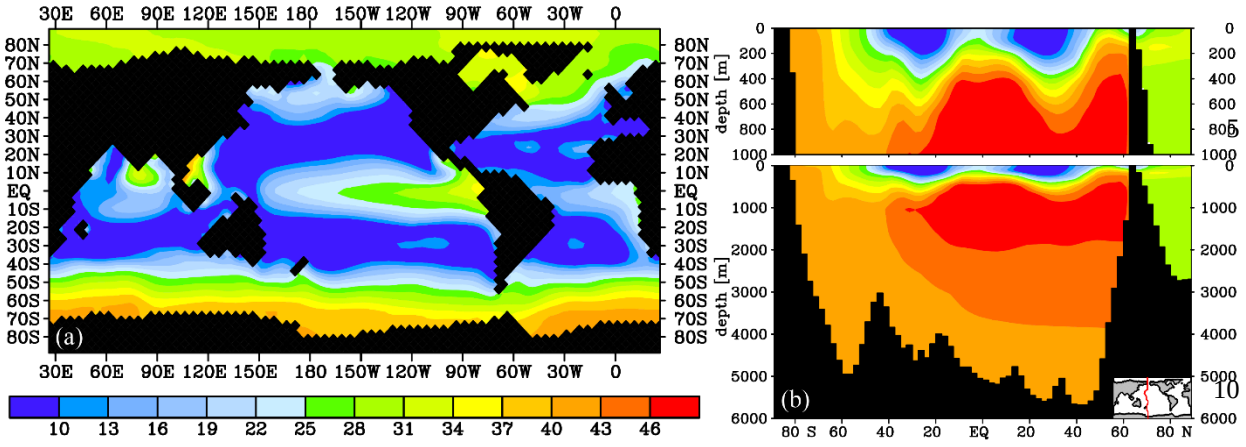

Figure 2 $\delta^{13}C_{bio}^{perc}$, the contribution of biology to the local $\delta^{13}C$ signal [%], as calculated using Eq. (4) at (a) 25 m depth and (b) a Pacific transect. The remainder of 100 % is attributed to air-sea gas exchange. The $\delta^{13}C$bio and $\delta^{13}C_{AS}$ values in ‰ are very similar to the values found by Schmittner et al. (2013).

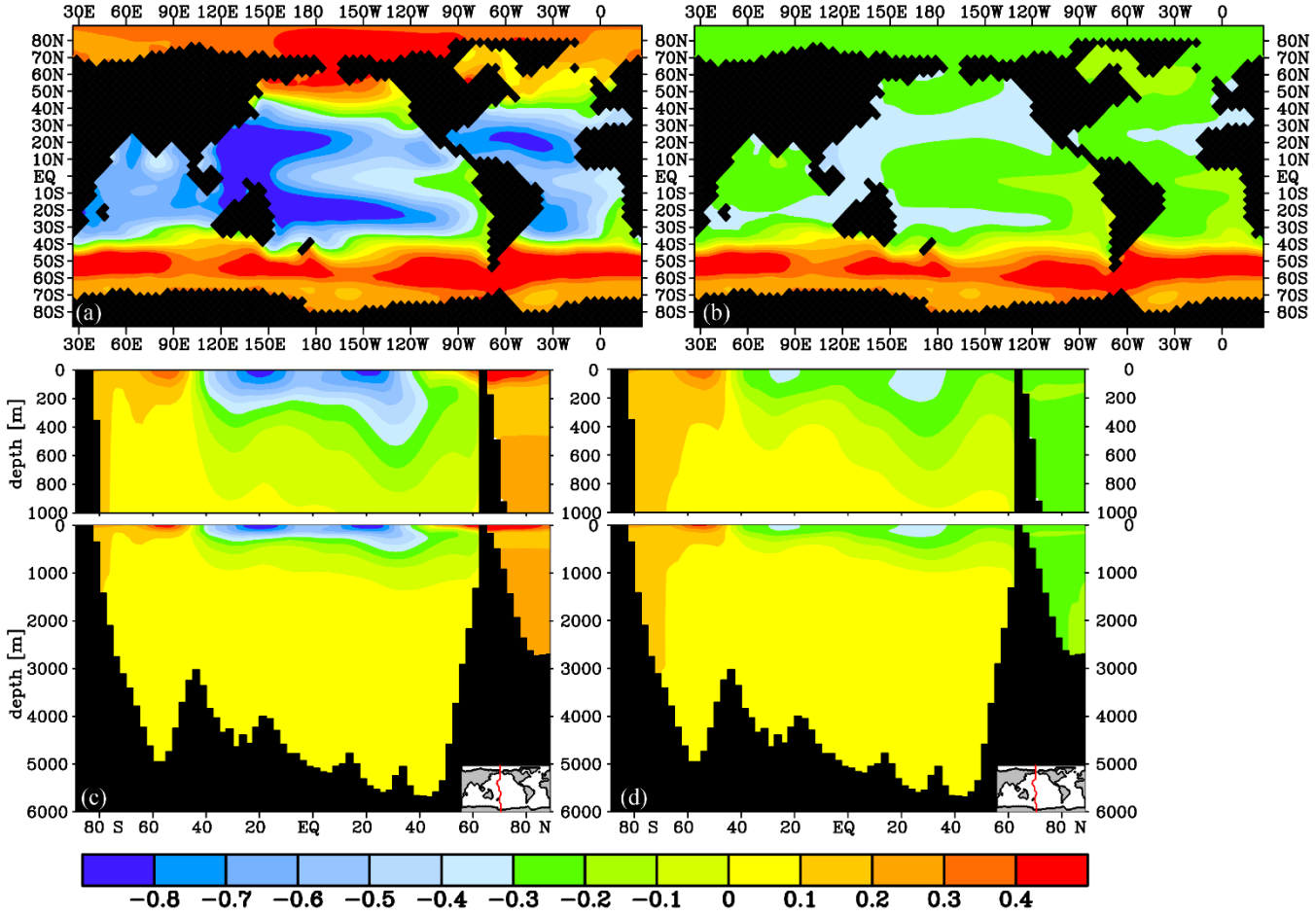

Figure 3 Modelled fast gas exchange sensitivity experiment $\delta^{13}C$ of DIC [‰] difference with the model control run: global experiments (a) and (c) and SO-only experiments (b) and (d), at 25 m depth (a) and (b) and as a Pacific transect of $\delta^{13}C$ difference (c) and (d).

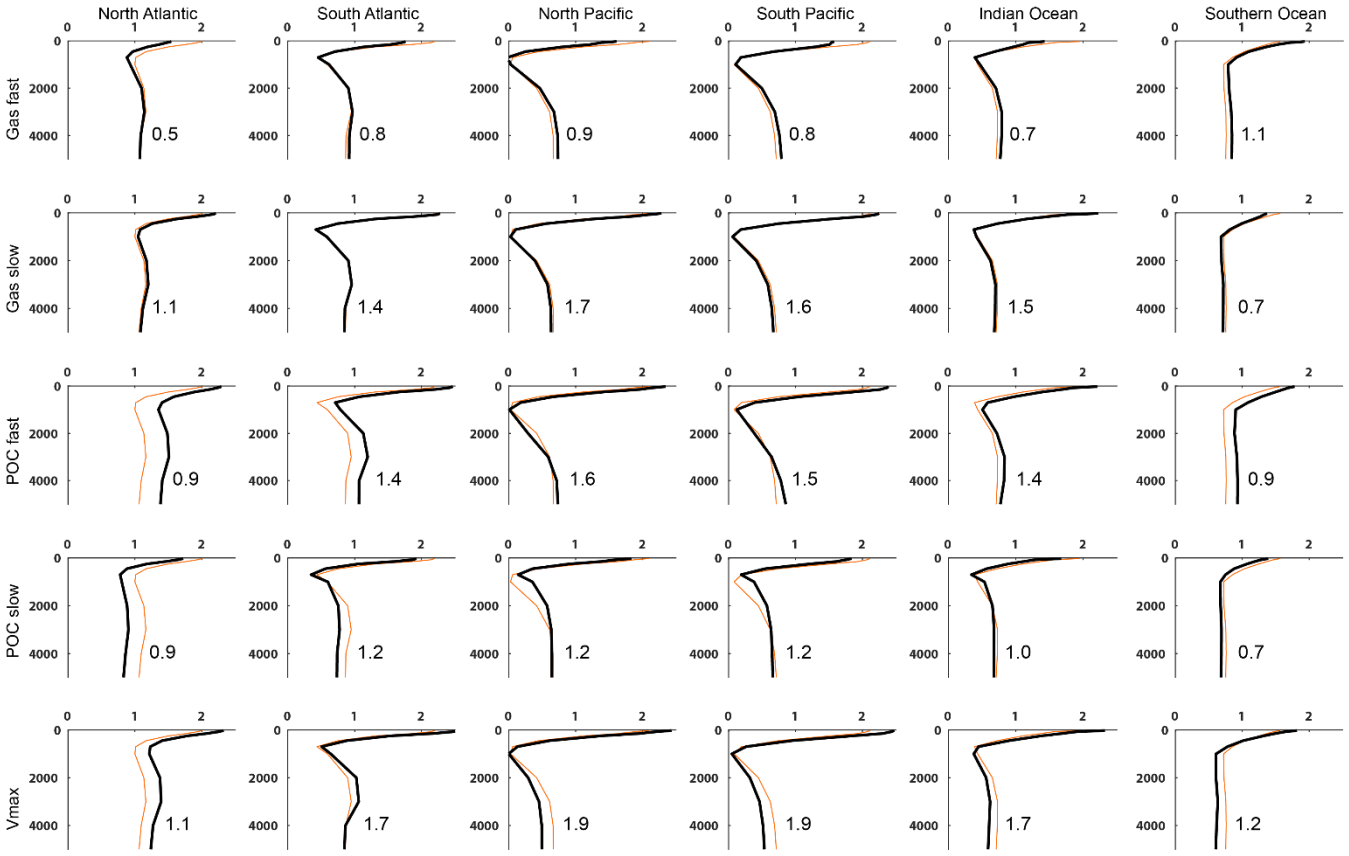

Figure 4 Volume-weighted basin mean profiles of $\delta^{13}C$, with $\Delta\delta^{13}C$ denoted per profile for the sensitivity experiments (thick black lines, Global for gas exchange and POC sinking experiments). Basin extent is visualised in Fig. S11. The thin orange line represents the control model run, which has a $\Delta\delta^{13}C$ of 0.9 (North Atlantic), 1.3 (South Atlantic), 1.4 (North Pacific), 1.4 (South Pacific), 1.2 (Indian Ocean) and 0.8 (Southern Ocean). See Fig. S7 for the resulting anomaly profiles for each experiment.

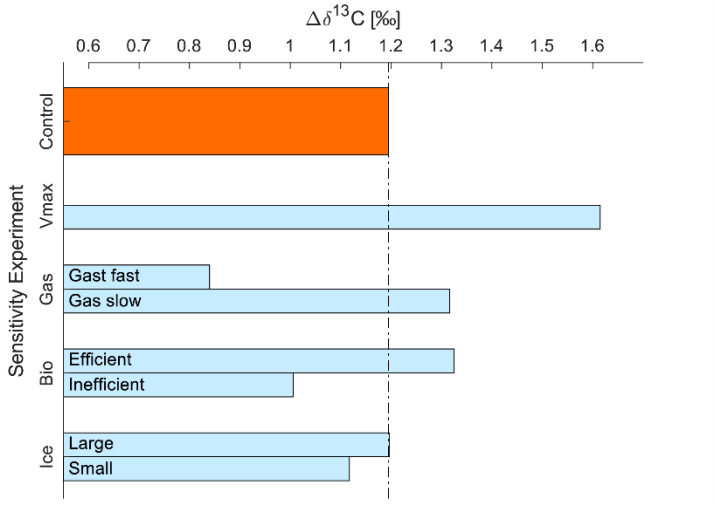

Figure 5 Global mean $\Delta\delta^{13}C$ for the different sensitivity experiments (Table 1). 'Bio Efficient' represents the high POC sinking rate experiment, 'Bio Inefficient' the slow POC sinking rate experiment. The results for the Southern Ocean only experiments (Sect. 2) are described in the text.

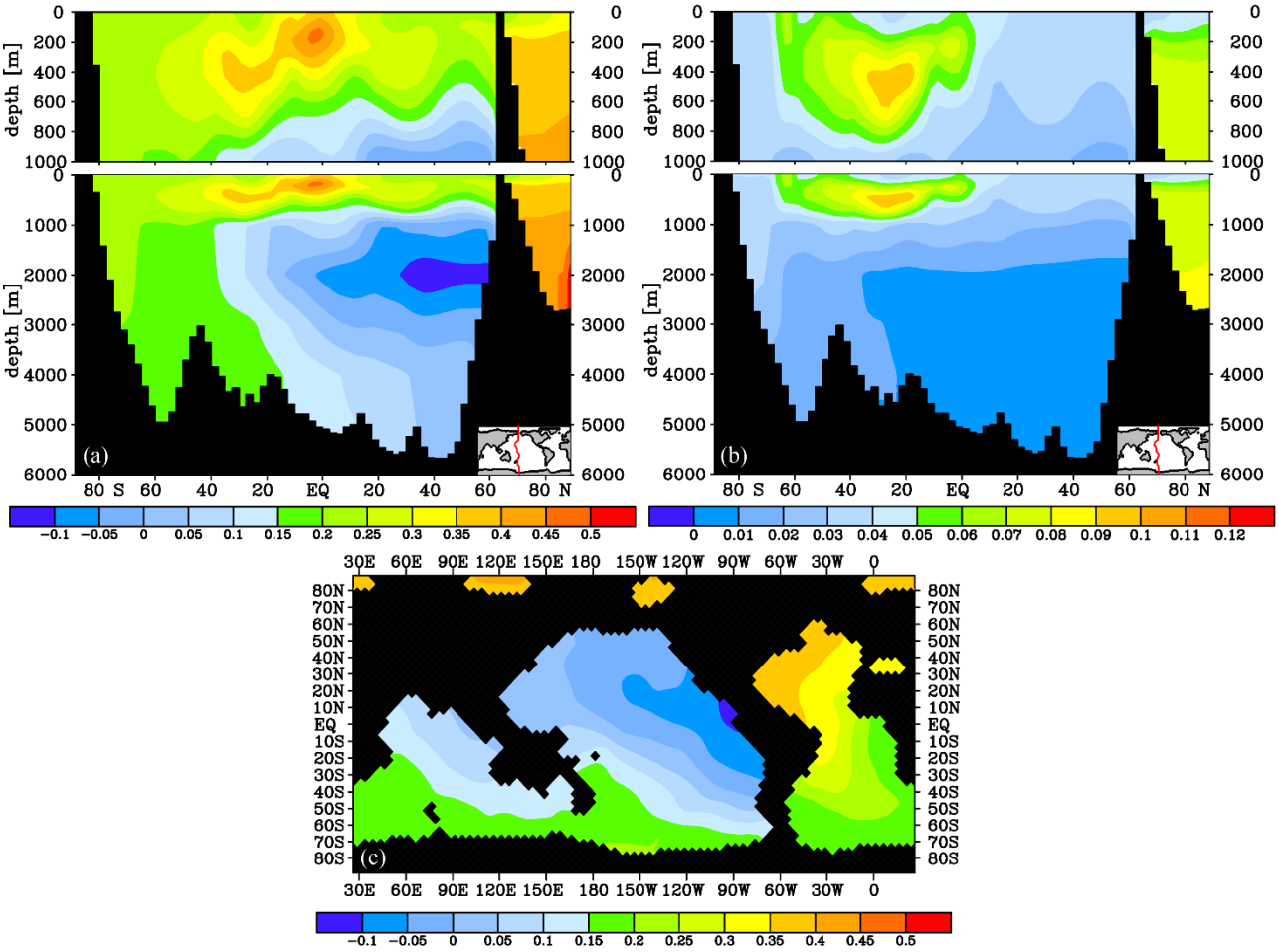

Figure 6 $\delta^{13}C$ of DIC difference between model control run and (a) the global efficient biological pump (high POC sinking rate) experiment for a Pacific transect and (b) the SO-only efficient biological pump (high POC sinking rate) experiment for a Pacific transect and (c) at 3000m depth for the global efficient biological pump experiment. Note the different scales.

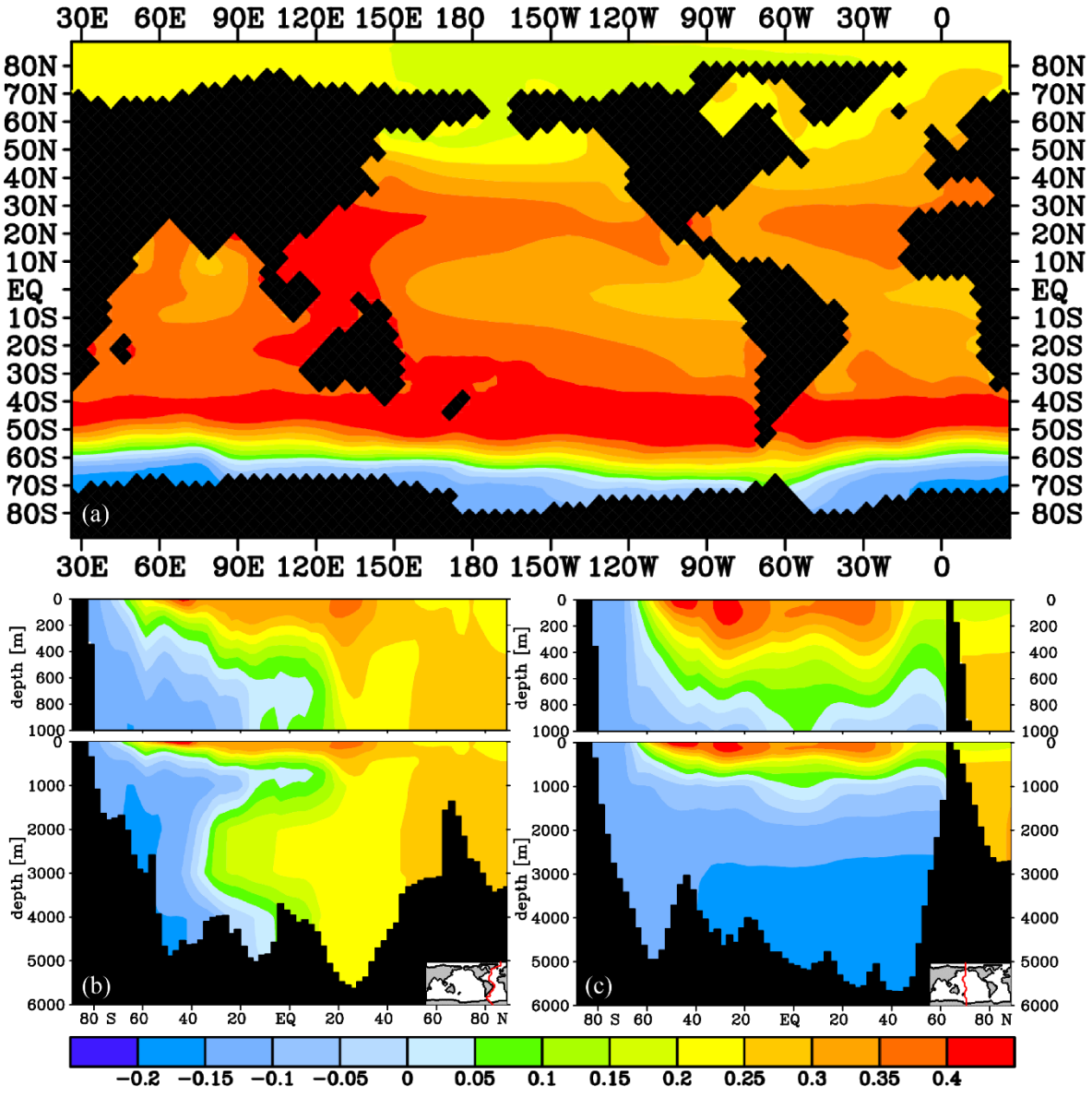

Figure 7 Difference plots between the model control run and the Vmax nutrient depletion experiment at (a) 25m depth and for (b) an Atlantic transect and (c) a Pacific transect.

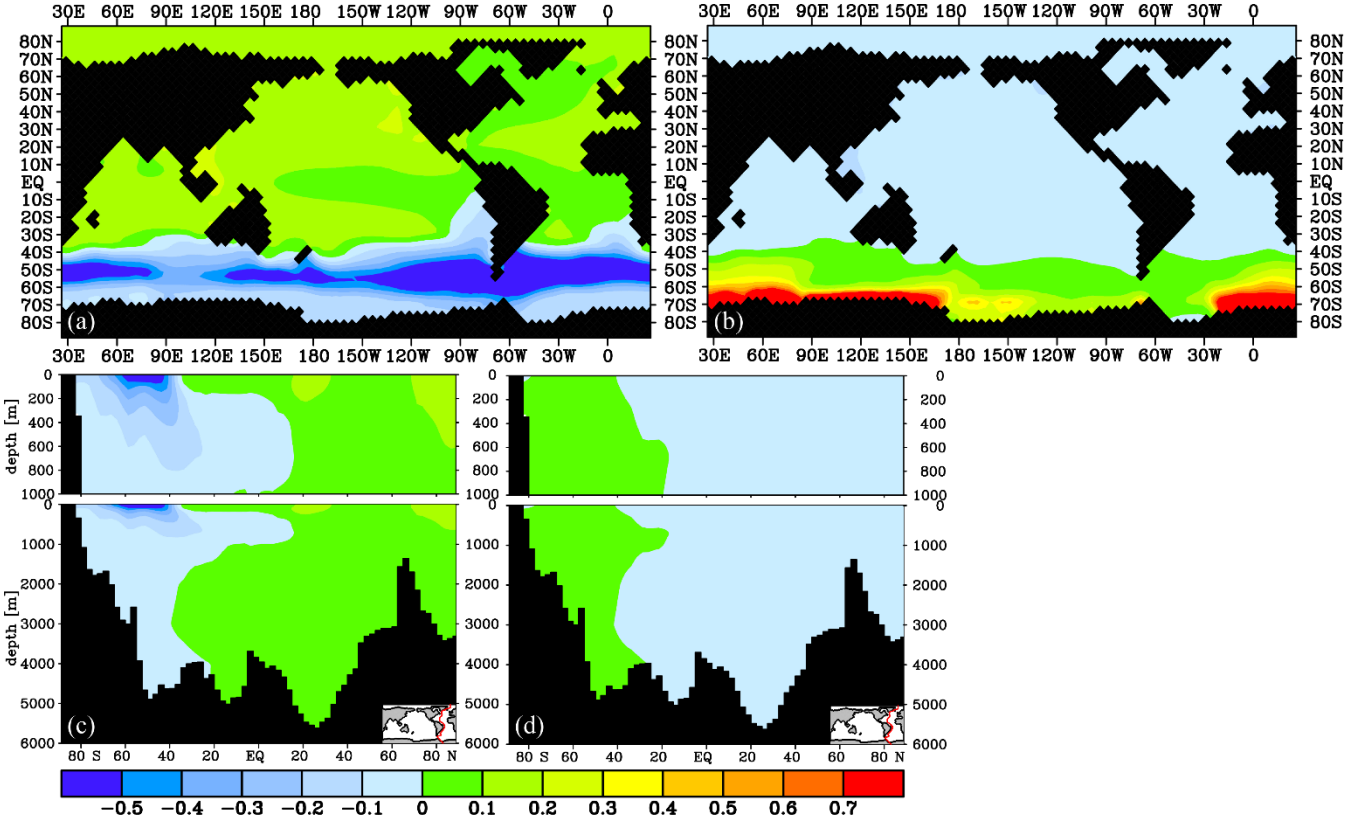

Figure 8 The effect of a large (a, c) and small (b, d) Antarctic sea ice cover on $\delta^{13}C$ as compared to the control for 25 m depth (a, b) and an Atlantic transect (c, d).

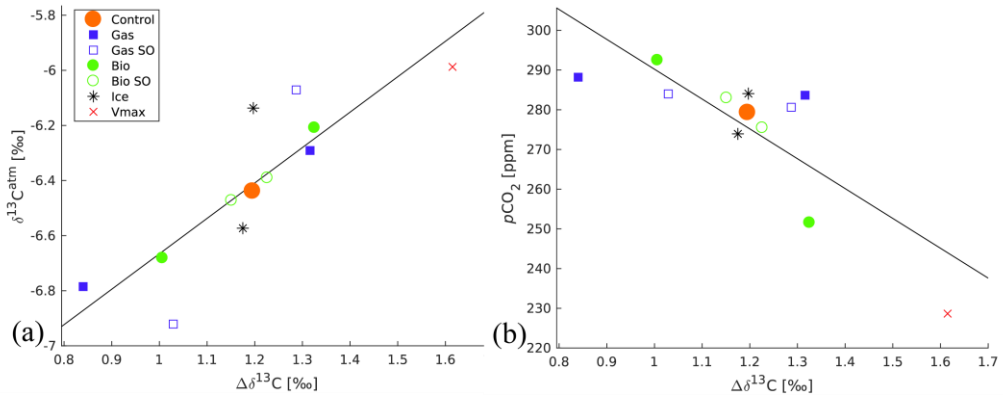

Figure 9 Scatter plot of the global mean $\Delta\delta^{13}C$ and (a) $\delta^{13}C^{atm}$ of the different sensitivity experiments. R-squared of the best-fit line is 0.73 (p-value 0.0004), and the line is described by y=1.3x-7.95 (b) pCO_2^{atm} of the different sensitivity experiments. R-squared of the best-fit line is 0.655 (p-value 0.00143), and the line is described by y=-75x+365.